

Investigating hydroclimatic impacts of the 168-158 BCE volcanic quartet and their relevance to the Nile River basin and Egyptian history

5 Ram Singh^{1,2}, Kostas Tsigaridis^{1,2}, Allegra N. LeGrande^{2,1}, Francis Ludlow³, Joseph G Manning⁴

¹ Center for Climate Systems Research, Columbia University, New York

² NASA Goddard Institute for Space Studies, New York, NY-10025

³ Department of History, School of Histories and Humanities, Trinity College, Dublin 2, Ireland

10 ⁴ Departments of History and Classics, Yale University, New Haven, CT 06520, USA

Correspondence to: Ram Singh (rs4068@columbia.edu)

Abstract.

The Ptolemaic era (305-30BCE) is an important period of Ancient Egyptian history known for its material and scientific advances, but also ongoing episodes of political and social unrest in the form of (sometimes
15 widespread) revolts against the Ptolemaic elites. While the role of environmental pressures has long been overlooked in this period of Egyptian history, ice-core-based volcanic histories have identified the period as experiencing multiple notable eruptions, and a repeated temporal association between explosive volcanism and revolt has recently been noted. Here we analyze the global and regional (Nile River Basin) climate response to a unique historical case of 4 consecutive and closely timed large, strato-volcanic
20 eruptions (first a tropical one, closely followed by 3 extratropical northern hemispheric events) between 168 and 158 BCE, a particularly troubled period in Ptolemaic history for which we now provide a more detailed hydroclimatic context. The NASA GISS ModelE2.1 Earth system model simulates a strong radiative response with a radiative forcing (top of atmosphere) of -7.5 W/m² (following the first eruption) and -2.5 w/m² (after each of the 3 remaining eruptions) at a global scale. Associated with this, we observe
25 a global surface cooling of the order of 1.5°C following the first (tropical) eruption, with the following three extratropical eruptions extending the cooling period for more than 15 years. Consequently, this series of eruptions constrained the northward migration of the inter-tropical convergence zone (ITCZ) during the northern hemisphere summer monsoon season, and major monsoon zones (African, South

Asian, and East Asian) experienced a suppression of rainfall of >1 mm/day during the monsoon (JJAS) season averaged for 2 years after each eruption. A substantial suppression of the Indian and north African summer monsoon (over the Nile River headwater region) strongly affected the modelled river flow in the catchment and river discharge at river mouth. River mass flow over the basin was observed to consecutively decrease by up to more than 30% relative to an unperturbed (non-volcanic) annual mean flow for 2 years after the tropical eruption. A moderate decrease of up to 10-20% was observed after each of the remaining eruptions. These results indicate, in sum, that the first eruption likely produced a strong hydroclimate response, with the following 3 eruptions prolonging this condition. These results also support the recent hypothesized association between ice-core-based signals of explosive volcanism and hydroclimatic variability during the Ptolemaic era, including the suppression of the agriculturally critical Nile summer flooding.

Key Words: Volcanic eruption, hydroclimate impacts, Inter-tropical Convergence Zone (ITCZ), Monsoon, Nile River basin

1. Introduction

Explosive volcanic eruptions that result in high altitude sulfate aerosol distribution across one or both hemispheres can diminish insolation with global and regional climatic impacts (e.g., Robock, 2000; Toohey et al., 2019). The sulfate aerosols resulting from (for example) the 1991 Mt. Pinatubo eruption of ~ 18 Tg SO_2 increased the atmospheric optical depth from ~ 0.6 to ~ 0.75 and was associated with surface cooling of 0.5 °C (Robock and Mao 1995; Parker et al., 1996). Volcanically induced cooling can also reduce net evaporation and hence precipitation over large areas (Lui et al., 2016; Iles et al., 2013), while also potentially producing a near global dynamical suppression of the northward migration of the inter-tropical convergence zone (ITCZ) during the boreal summer, as the convergence follows the surface area of maximum temperature (Pettersen et al., 2000; Chiang and Bitz, 2005; Broccoli et al., 2006; Colose et al., 2016). These changes can impact river outflow (Oman et al., 2006; Sabzevari et al., 2015; Kostiç et al., 2016) with implications for civilizations from antiquity to the present-day. The Nile River, upon which

Egyptian agriculture was heavily dependent, is a key example. With ice-core-based volcanic histories now identifying several hundred potentially climatically effective eruptions over the past 2.5 millennia (Sigl et al., 2015), Egyptian civilization provides a test-case for the study of human vulnerability to abrupt environmental changes in having experienced repeated volcanically induced “hydroclimatic shocks”
60 (e.g., Mikhail, 2015; Manning et al., 2017, 2021).

Explosive volcanic eruptions represent the major natural source of forced variability in the climate system at yearly to decadal time scales (Schmidt et al., 2011; Colose et al., 2016; Swingeduow et al., 2017; Khodri et al. 2017). Powerful explosive eruptions can inject sulfur-rich gases into the stratosphere, where they oxidize to form sulfate aerosols that can persist for months to years, impacting climate on regional to
65 global scales. Volcanic stratospheric aerosols can cause troposphere cooling by scattering incoming shortwave radiation, while also heating the stratosphere (Robock and Mao, 1992). Unequal north-south stratospheric heating due to volcanic aerosols concentrated in lower latitudes after tropical eruptions can influence major modes of circulation and surface climate variability such as the Arctic Oscillation/North Annular Mode (AO/NAM) and North Atlantic Oscillation (NAO), driving an enhanced westerly airflow
70 (Shindell et al., 2004; Zanchettin et al., 2021). The post-volcanic surface temperature response can affect the El Niño/La Niña phase and Southern Oscillation and have a long-term impact on Atlantic Meridional Overturning Circulation (AMOC) strength (Khodri et al., 2017; Wahl et al., 2014; Robock and Mao, 1995; Pausata et al., 2015). Extratropical eruptions are usually thought to have a weaker impact than tropical eruptions. This arises in part because of the background Brewer-Dobson circulation upwelling in
75 the tropics and downwelling at higher latitudes, which affects the stratospheric lifetime of volcanic aerosols (Kirtman et al., 2013; Myhre et al., 2013; Schneider et al., 2009). Recent studies have, however, illustrated the potential for a dynamically induced and disproportionately strong climate forcing from such eruptions (Toohey et al. 2019).

Volcanic injection of sulfur-containing compounds can, too, influence stratospheric chemistry, yielding
80 further complex atmospheric and climatic responses upon interacting with water and halogens (LeGrande et al., 2016; Brenna et al., 2020; Staunton-Sykes et al., 2021). Paleoclimate records and climate modeling suggest that the dynamical response to volcanic aerosol causes a net (but regionally variable) drying and impacts global rainfall patterns (PagesHydro2k/Smerdon et al., 2017; Colose et al., 2016; Liu et al., 2016;

Iles and Hegerl, 2014). Trenberth and Dai (2007) thus analyzed the impact of the Pinatubo (1991) eruption
85 on terrestrial precipitation and river streamflow and found an increase in associated drought conditions in
1992. Joseph and Zeng (2011) suggested that volcanically induced rainfall anomalies over land and ocean
can seasonally modulate tropical drought. Hemispheric biases in volcanic aerosol distribution can,
moreover, impact the movement of ITCZ by constraining its summertime migration into the energetically
deficit hemisphere (Colose et al., 2016; Xian and Miller, 2008). Effectively, the ITCZ shifts “away” from
90 the hemisphere with the greatest aerosol burden. For tropical eruptions, even those producing roughly
even hemispheric burdens, this movement is typically more southward owing to the larger amount of land
in the Northern Hemisphere and relative the greater ocean area (and higher thermal capacity) of the
Southern Hemisphere.

For Africa, eruptions producing asymmetrical latitudinal aerosol burdens (e.g., Katmai in 1912, El
95 Chichón in 1982) may have enhanced 20th century Sahelian droughts by influencing the strength and
position of Hadley cells (Haywood et al., 2013). Of the Nile, monsoon rainfall over the Ethiopian
highlands contributes (via the Blue Nile and Atbara River) ~85% to the summer flood in Egypt and is a
strong control on its interannual variability (Melesse et al., 2011). Ancient Egypt was famed for the
productivity of its flood recession agriculture, but the Nile summer flood was also famously variable, with
100 insufficient flooding impacting Egyptian society (e.g., Bell, 1975; Butzer, 1976, 1984; Said, 1993;
Hassan, 1997a, b; Hassan, 2007; McCormick, 2013). Some of this variability was driven by explosive
volcanism. The Laki fissure eruption (1783/84) injected approximately 122 Mt of SO₂ into the atmosphere
over eight months, producing a strong cooling and suppressing the African monsoon (Oman et al., 2006;
D’Arrigo et al., 2011). The resulting diminished Nile flooding (Oman et al., 2005, 2006; Mikhail, 2015)
105 is known colloquially as “Nile failure”. Similar impacts were simulated and can be observed for the
Katmai (1912) eruption (Vorosmarty et al., 1998; Thordarson and Self, 2003; Oman et al., 2005, 2006;
Manning, 2018).

The most richly documented period of ancient Egyptian history is the Ptolemaic era, 305-30 BCE, with
Egypt ruled by Greeks in a lineage beginning with Ptolemy I Soter (d. 283 BCE), previously one of
110 Alexander the Great’s key generals and instrumental in Egypt’s conquest. The period distinguishes itself
for mixing Greek and Egyptian traditions, its material, cultural and scientific achievement (e.g., the

founding of Alexandria with its Great Library), but also its chronic political instability (McGing, 1997; Ludlow and Manning, 2016; 2021). External environmental influences have been little considered in this, despite the dependence of Egyptian agriculture on the summer flood. However, recent work has revealed

115 a repeated close coincidence in the timing of many (if certainly not all) internal revolts and ice-core-based dates of inferred-tropical and NH extratropical eruptions that appears statistically significance (i.e., non-random) (Ludlow and Manning, 2016, 2021; Manning et al., 2017). One example is the “Great Theban Revolt” starting in c.207 BCE, shortly after a 209 BCE tropical eruption (Sigl et al., 2015), with extensive territories lost to two native Pharaohs (Ludlow and Manning, 2016; Ludlow et al., 2023).

120 That the revolt and eruption dates under study derive from independent chronologies (documentary and ice-core) helps exclude potential biases in estimating this statistical significance. For example, inflated correlations may result between events known from the same sources (e.g., between extreme weather and societal stresses such as famine, if those instances of extreme weather that contributed to such stresses were more likely to have been documented than those that didn’t (White and Pei, 2020)). It is a truism

125 that correlation does not establish causation. Genuine causality is, however, implied where significance testing suggests an observed correlation is unlikely to have arisen randomly, though this does not determine the direction or character of causality (Izdebski et al., 2023). Statistical significance may, moreover, be sensitive to many factors. These include here (1) the choice of statistical test, (2) the choice of revolt and eruption dates (if uncertainties exist), (3) judgements as to what constitutes “revolt” (vs.

130 phenomena like food riots motivated more by desperation than politics), and (4) judgements concerning which eruptions to include in testing (e.g., seeking those with a meaningful impact vs. non-climatically effective eruptions introducing “noise” into the analysis), assessed by estimated volumes and heights of atmospheric SO₂ injections, eruption locations, and more. Notably, thus, testing by Ludlow and Manning (2016) was followed by Manning et al. (2017) who also observed a statistically significant coincidence

135 between eruptions and Ptolemaic-era revolts using different methods and variant dates.

Logic dictates that the direction of any genuine causality must flow here from eruption to revolt (Izdebski et al., 2023). Further confidence in its reality arises from the existence of plausible mechanisms connecting volcanic hydroclimatic variability with revolt (i.e., via reduction of the Nile summer flood and consequent societal impacts). Much work remains to further characterize this causality, how direct or

140 indirect it may have been, and whether this changed meaningfully through time (and between revolts that varied in geography and scale) according to (or in interaction with) other coincident potential causes (from longer term developments promoting chronic vulnerabilities, to more acute political and socioeconomic stresses). White and Pei (2020) argue that such questions represent a key challenge for climate historians and related scholars, recommending a framework wherein potential causes are assessed using a
145 framework of necessary and sufficient conditions (put simply; see also Ludlow et al. (2023)). Gao et al. (2021) employ a framework wherein the role of volcanically induced hydroclimatic “shocks” in the collapse of Chinese dynasties is characterized along a spectrum from “ultimate” to “proximate” causation (see also Villmoare (2022) for this framework). Here, smaller hydroclimatic shocks could act as the ultimate cause of collapse when enabled by high pre-existing stress, while larger shocks could act with
150 greater independence as proximate causes without substantial pre-existing stress.

An alternative framing in many climate-conflict studies (not incompatible with that proposed by White and Pei (2020) or employed by Gao et al. (2021)) is to delineate multiple identifiable “pathways” that may enable or lead (through material (economic), political, cultural or psychological channels) to links between hydroclimatic variability and various forms of conflict (see Hsiang and Burke (2014) and Ide
155 (2017) for reviews). Success here requires that statistical findings are interpreted with due reference to the relevant historical, political, geographical contexts. For Ptolemaic Egypt, one hypothesized pathway involves the societal impacts and responses to sudden hydroclimatic variability that can follow explosive volcanism, and influence (alongside other regional factors) the intensity of the African monsoon. When this causes a “failure” of the Nile summer flood, many adverse societal impacts may occur. These include
160 harvest failure (seen also in other periods of Egyptian history (e.g., Hassan, 1997a,b; Mikhail, 2015)), possibly prompting subsistence-driven migration to urban areas, with inability to meet state taxation demands (payable in grain) also potentially necessitating the sale of hereditary familial lands (Manning, 2003; Manning et al., 2017). These stressors might work in tandem with the psychological and religious significance of a “failed” flood, something widely feared, and which could be interpreted (even
165 propagandized to foment revolt) as signaling divine displeasure at the Pharaoh (Ludlow and Manning, 2021; Ludlow et al., 2023). In the Ptolemaic context, when some native Egyptian elites were likely

resentful of Greek rule, with taxation and other advantages given to those of Greek backgrounds (McGing, 1997; Ludlow et al., 2023), a Nile failure may have held particular political potency.

170 Huhtamaa et al. (2022) have called for case studies of the hydroclimatic and socioeconomic impacts of specific eruptions to advance understandings of human-environmental causalities. For Ptolemaic Egypt, the 160s BCE are particularly relevant in experiencing considerable internal revolt and instability. Indeed, the Ptolemaic dynasty might have fallen here without self-interested Roman intervention against the Seleukid empire (rivals to the Ptolemies) after their invasion (170-168 BCE) of Egypt under King Antiochus IV (Grainger, 2010; Blouin, 2014; Manning et al., 2017). This period is also remarkable for 175 three notable volcanic eruptions (168, 164, 161 BCE), with another in 158 BCE (Sigl et al., 2015), which we term the “eruption quartet”. Substantial sulfate across both poles identifies the first (168 BCE) as the largest and likely tropical, followed by three moderate eruptions in the northern hemisphere extratropics (Sigl et al., 2015). While high-resolution paleoenvironmental proxies for Egypt are effectively absent for this period, the hydroclimatic impacts of these eruptions can be explored by climate modeling.

180 Few studies have examined the climatic-societal effects of eruption clusters. These include the cluster between 1108 and 1110 CE (Guillet et al., 2020), the “double event” of the 6th century in 536 and 540 CE (Toohey et al., 2016), and the cluster from 1637 to 1641 (Stoffel et al., 2022; Huhtamaa et al., 2022). These studies variously employed paleoclimatic data, written evidence and/or climate modelling to reveal strong negative post-eruption temperature anomalies for the Northern hemisphere, thereby suggesting the 185 potential for diminished crop yields and providing a climatic context to better understand the human history of these periods. Here, we intend to advance our understanding of the likely hydroclimatic impact of the 168-158 BCE eruption quartet as a foundation for ongoing efforts to more securely establish and qualify the causality underlying the observed association between eruptions, Ptolemaic-era revolts, and other political and socioeconomic phenomena and developments.

190 We thus use a computationally expensive but more sophisticated version of the National Aeronautics and Space Administration (NASA), Goddard Institute for Space Studies (GISS) Earth system model, GISS ModelE2.1-MATRIX (Bauer et al., 2008; Bauer et al., 2020), to simulate the 168-158 BCE eruption quartet and regional hydroclimate responses over the Nile River basin. Section 2 presents model details and experiment methodology. Estimation of background climate for the 2.5k period (orbital and

195 greenhouse gases (GHGs) changes), alongside impacts due to PMIP4 (Paleoclimate Model Intercomparison Project, phase 4) vegetation cover estimates for the period are considered in section 3. Particular subsections evaluate the GISS ModelE for its capability to resolve the microphysical properties of volcanic aerosols during this period and to analyze the radiative impacts of the aerosols from these eruptions, which control their radiative and hydroclimatic impacts (Timmreck et al., 2009; Timmreck et al., 2010; Schmidt et al., 2010). The discussion and conclusion (section 4) summarize our results and
200 al., 2010; Schmidt et al., 2010). The discussion and conclusion (section 4) summarize our results and considers how they can advance understandings of the period's fraught history in Egypt.

2. Methodology & Experiment design

2.1 Model Description

205 We used the NINT (Non-INTeractive) version (Kelley et al., 2020) of GISS ModelE2.1 to simulate background climate conditions corresponding to 2500 years before present (2.5ka, kilo-years BP), similar to protocols for the mid-Holocene (6ka) coordinated experiment (Kageyama et al., 2017), but adjusting trace gases and orbital forcing for 2.5ka. The term “non-interactive” means that atmospheric composition and climate are decoupled, so any changes in composition are handled by external input only. Once our
210 model attained an equilibrium climate state, we enabled atmospheric composition-climate interactions for our experiments, described below.

GISS ModelE2.1 is a state-of-the-art Earth System Model contributing to the Climate Model Intercomparison Project (CMIP) phase 6 (Eyring et al., 2016). The model's atmospheric component simulates on a horizontal resolution of 2° latitude by 2.5° longitude with 40 vertical layers and a model
215 top at 0.1 hPa. It is coupled to the GISS Ocean v1 model at a horizontal resolution of 1° latitude by 1.25° longitude with 40 layers. The Demographic Global Vegetation Model (DGVM) is the Earth Terrestrial Biosphere Model (TBM) (Kiang, 2012; Kim et al., 2015) and was used to implement climate-influencing vegetation properties, including satellite-driven (MODIS) plant functional types (PFTs) and the monthly varying leaf area index (LAI) (Gao et al., 2008; Myneni et al., 2002). Tree heights come from Simard et al. (2011) and include an interactive carbon cycle (Ito et al., 2020). The MATRIX (Multiconfiguration
220 Aerosol TRacker of mIXing state) aerosol microphysics module (Bauer et al., 2008; 2020) was used in

our coupled composition-climate runs to simulate the active volcanism and corresponding climate conditions. MATRIX is an aerosol microphysics scheme using the quadrature method of moments, representing new particle formation (Vehkamäki et al., 2002), aerosol-phase chemistry, condensational growth, coagulation and the mixing state of aerosols (Bauer et al., 2013). MATRIX tracks 16 mixing states with 51 aerosol tracers and resolves mixtures of sulfate, nitrate, ammonium, aerosol water, black carbon, organic carbon, sea salt and mineral dust (Bauer et al., 2008). MATRIX includes the direct effect and the first indirect effect of aerosols on climate.

Approximate eruption locations are crucial to estimate climatic impacts (Toohey et al., 2016, Aquila et al., 2018 [https://acd-ext.gsfc.nasa.gov/Documents/NASA_reports/Docs/VolcanoWorkshopReport_v12.pdf]). Locations for the 168-158 BCE eruptions were first chosen following the bi-polar multi-ice-core sulphate deposition data of Sigl et al. (2015), which allow a discrimination between likely tropical (low-latitude) eruptions and those likely in the extratropics of either hemisphere. Without additional data (e.g., ice-core tephra) providing more precise locations, the ultimate model location must be selected more arbitrarily. Our chosen locations are shown in Fig S3, and we note that eruption longitude (versus latitude) is not expected to play a major role as an uncertainty factor in the modelled climatic response. The forcing potential of each eruption in terms of atmospheric SO₂ injection was also estimated using the Sigl et al. (2015) multi-ice-core record of sulfate deposition over Greenland and Antarctica, linearly scaled corresponding to Pinatubo (1991) eruption estimates of 18.5 Tg SO₂ (Wolfe and Hoblitt, 1996). Injection height was selected to match Pinatubo, absent further information.

2.2 Experiment Design

A control simulation for the 2.5ka period was performed using the PMIP phase 4 protocols for the mid-Holocene (6ka) experiment, altered for conditions appropriate to 2.5ka. This included altering the orbital forcing, greenhouse gases (CO₂: 279 ppm, N₂O: 266 ppb, and CH₄: 610 ppb), plus vegetation in Africa and high boreal Eurasia and North America (Otto-Bliesner et al., 2017). Ozone and aerosols were prescribed to non-anthropogenic conditions only – this is distinct from pre-industrial simulations that do include small anthropogenic changes and attendant aerosol and atmospheric chemistry changes. Orbital

and greenhouse gas forcings for the 2.5ka period are expected to play a vital role in producing the correct
250 equilibrium climate. We ran a control run with the NINT configuration for 1000 years to get the model
in equilibrium, then extended this for 100 years by adding the MATRIX version of ModelE2.1 to again
achieve an equilibrium state for a 2.5ka period with composition-climate interactions enabled. Vegetation
cover, LAI and vegetation height were prescribed corresponding to the piControl period climate. A lack
of exact vegetation cover information prevents GCMs without dynamic vegetation model from
255 reproducing mid-Holocene warm Northern hemisphere summer and enhanced NH monsoons conditions
(Tierney et al., 2017; Larrasoana et al., 2013). However, the vegetation cover used here as defined by the
PMIP4 protocol vegetation sensitivity experiment (Otto-Bliesner et al., 2017) for the mid-Holocene
period shows an intense impact on North African rainfall and explains the difference between simulated
and reconstructed climate conditions (Braconnot et al., 1999; Pausata et al., 2016). To address this, we
260 created a modified mid-Holocene boundary condition sensitivity vegetation map by linearly interpolating
between pre-industrial vegetation and the Mid-Holocene vegetation sensitivity experiment (i.e., northern
hemisphere high latitude tundra during the pre-industrial was replaced by boreal forests, while African
vegetation was altered with evergreen shrubs replacing all vegetation up to 25N and grasslands up through
the Mediterranean Coast in 6ka (Otto-Bliesner et al., 2017)).

265

Fig S1 (Supplementary Information) shows the major vegetation plant function type (PFT) cover changes
under the PMIP4 sensitivity vegetation protocols after linearly interpolating for the 2.5ka period. The
2.5k equilibrated simulation with MATRIX was then extended for 70 more years with a corrected dust
tuning (a typical process when equilibrating the model on a new climate state), and a further 130 years
270 with the linearly interpolated PMIP4 vegetation described above (see table TS1 for details of control runs
and annual global mean time series of surface air temperature and precipitation in Fig. S2). This run
equilibrated very quickly and no further tuning was needed. We thus used the last 100 of the total 130
years of that equilibrated run as the base climate for our analysis. An ensemble of 10 members with active
volcanic eruptions was simulated using a restart file every 10 years during the last 100 years of the control
275 simulation corresponding to 2.5ka period as summarized in table TS1, following the same approach as
performed for the CMIP6 ensemble simulations (Kelley et al., 2020).

The starting timepoint for each ensemble member is shown by blue vertical lines in fig S2. Each member started January 1st of the year 169 BCE and ran for 16 years, with each eruption happening on the 15th of June of the 2nd, 6th, 9th and 12th years modelled. Because exact eruption dates cannot be determined from ice-core sulphate deposition data, due to ice-core chronological uncertainties and lags between eruptions and the deposition of sulphate in the ice, we selected a summer eruption date to investigate impacts on northern hemisphere monsoon and wintertime atmospheric circulation. We also note that modelling accuracy will depend partly upon the accuracy of the ice-core-based forcing reconstruction employed. Uncertainties can arise, for example, because of variation in sulphate deposition across the polar regions for any given eruption. It is thus notable Sigl et al. (2015) employ several Antarctic and Greenland ice-cores in their reconstruction, helping to average out regional variability in deposition, but our results can be revisited as reconstructions incorporate more ice-cores.

Table 1. Details of eruptions applied in this experiment, with each eruption happening on the 15th of June of the 2nd, 6th, 9th and 12th model years.

Eruption	Year (BCE)	Position	Eruption injection (SO ₂)	Injection Height (km)
E1	168	Pinatubo (15.13, 120.35) (Tropical)	22.5 Tg	22-26
E2	164	Mt Laki, Iceland (64.03, -18.13 W) (NH)	6.5 Tg	22-26
E3	161	Mt Katmai, Alaska Peninsula (58.28, -154.95 W) (NH)	7.2 Tg	22-26
E4	158	Shiveluch, Kamchatka, Russia (56.39, 161.21) (NH)	7.5 Tg	22-26

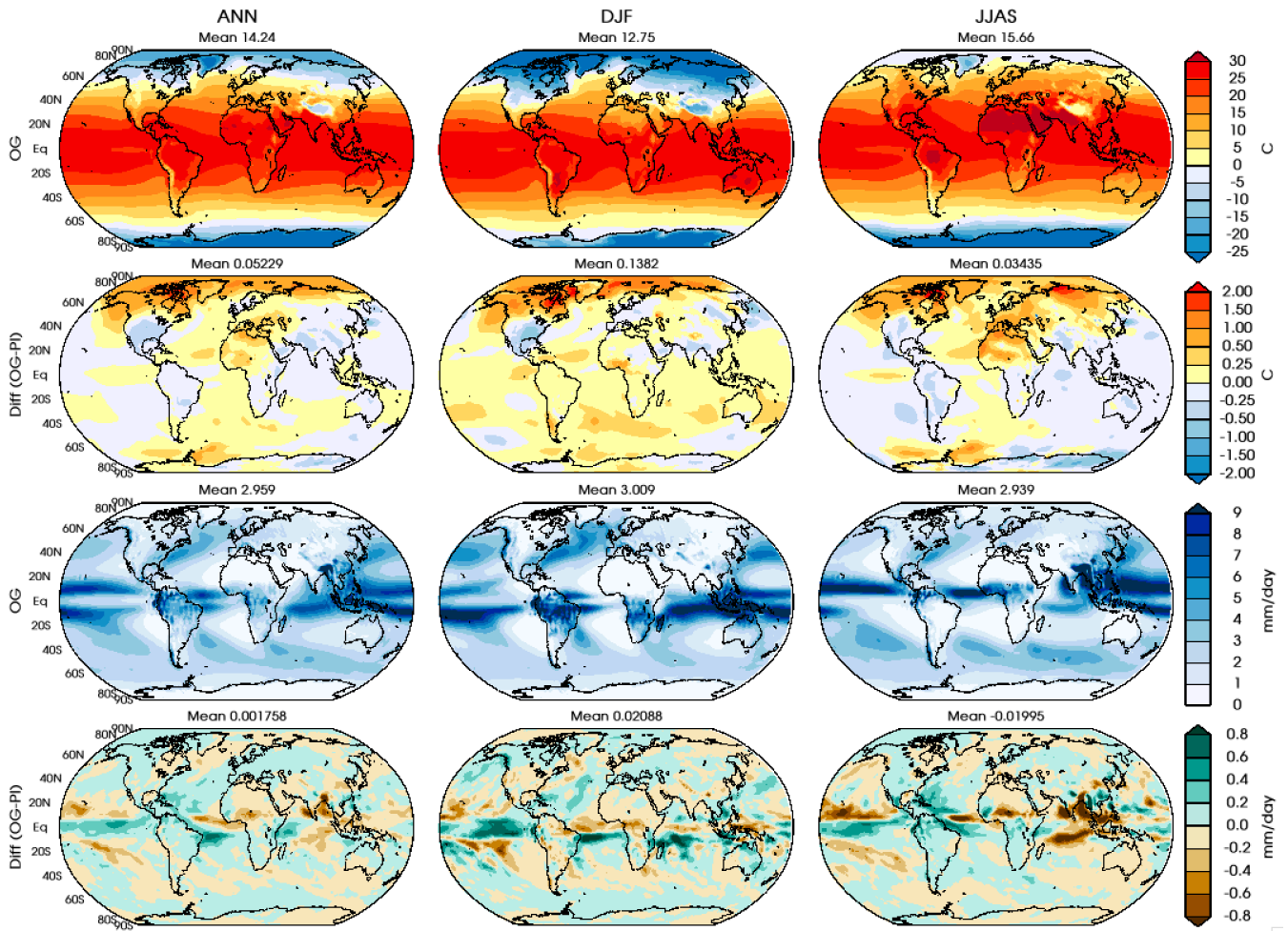
3. Results

3.1. 2.5ka control runs

295 We first evaluated the 2.5ka control climate run for providing a precise background climate to investigate the impacts of the 168-158 BCE volcanic quartet.

3.1.1 2.5Ka GHG+ORB climate

We compared the 2.5ka equilibrium climate with only GHG, orbital, and non-anthropogenic forcing changes against a preindustrial (year 1850) control run to evaluate the impact (alone) of orbital and greenhouse gas changes on our base climate state. Surface air temperatures showed globally minimal differences with a warming of northern hemisphere high latitudes due to the different orbital forcing for all seasons (Fig 1). The implications of changes in orbital forcing for 2.5k are thus evident in the surface temperature but the northern hemisphere monsoon season (JJAS) and winter season (DJF) rainfall slightly was reduced along the northern equatorial belt. This points to the limitation of the GISS model in not having an interactively dynamic vegetation component to reproduce the known mid-Holocene wet African landcover conditions (Harrison et al., 2015; Tiwari et al., 2022). Numerous studies have demonstrated that including bio-geophysical feedbacks and atmospheric dynamics helps to successfully model the wet African conditions for mid-Holocene (Kutzbach et al., 1996; Claussen et al., 2003; Kutzbach and Liu, 1997; Hewitt and Mitchell, 1998). Using PMIP4 vegetation over northern hemispheric regions is known to provide a solution to the same long-standing issue with CMIP3/CMIP5 models that fail to reproduce these wet African conditions for mid-Holocene (Harrison et al., 2015).

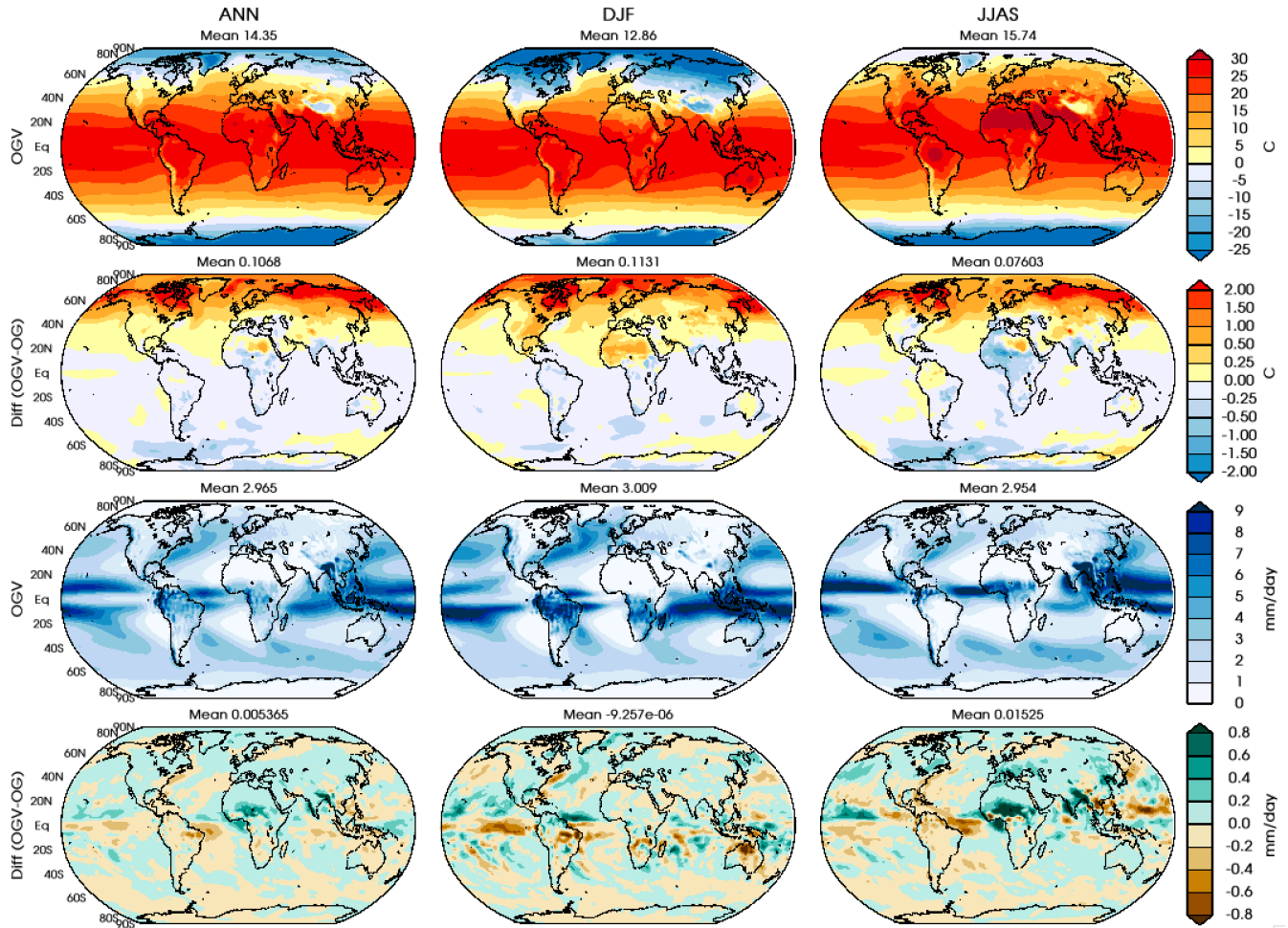


315 Fig 1. Seasonal mean (Annual, DJF & JJAS) surface air temperature (top row) for 2.5k period equilibrium
 run, differences from the preindustrial period (2.5ka-preindustrial) for all three seasons (2nd row from top)
 and seasonal (Annual, DJF & JJAS) mean precipitation (3rd row from top) and the difference (bottom
 row) from preindustrial period (2.5ka-preindustrial). The equilibrium run for the 2.5k period includes the
 orbital and GHG concentration changes for the 2.5k period (referred to as OG), the preindustrial period
 (as PI), and their difference (OG-PI) as simulated by GISS ModelE2.1.

320

3.1.2 2.5Ka ORB+GHG+VEG climate

The comparison of mean climate for the 2.5ka period for inclusion of PMIP4 vegetation is shown in fig 2 for the mean surface air temperature and precipitation for the Annual, DJF and northern hemisphere monsoon (JJAS) seasons.



325

Fig 2. Mean surface air temperature for Annual, DJF and JJAS seasons (top row) and seasonal mean precipitation (3rd row from top) for the equilibrium runs with the PMIP4 vegetation for the 2.5k period and surface temperature difference (2nd row from top) plus the seasonal precipitation differences (bottom row) for the 2.5k period as simulated by GISS ModelE2.1. We have used a short initial notation for our for forcings to denote the difference (ORB+GHG+VEG = OGV and ORB+GHG= OG)

330

GISS ModelE2.1 simulated a global a mean surface air temperature (SAT) of 14.4 °C, 12.8 °C and 15.7 °C for Annual, DJF and JJAS seasons respectively for the 2.5ka (ORB+GHG+VEG) simulation, which is

0.11 C (Annual), 0.11 °C (DJF) and 0.08 °C (JJAS) higher than the 2.5ka (ORB+GHG) simulation without including these vegetation changes. A strong increase in surface air temperature of greater than 2°C was calculated for northern hemisphere high latitude land regions, particularly where landcover (tundra) was replaced by boreal forest, decreasing ground surface albedo during snowy winter months. A moderate rise of 0.5°C was also simulated for Africa, coinciding with regions of vegetation changes (described in section 2.2). The regional pattern of difference in rainfall in the northern hemisphere monsoon season (JJAS) was observed mostly over the North African and Asian regions. The observed increase of 0.4 mm/day or greater over the North African and Southwest Asian monsoon regions indicates a northward movement of the ITCZ during the monsoon season, consistent with expectations given the modified vegetation for this period and in agreement with current understanding of mid-Holocene rainfall regimes (Tierney et al., 2017; Tiwari et al., 2022). These results also acknowledge the sensitivity of the hydroclimatic impacts to regional landcover and hydrological conditions (Singh et al., 2020).

We also analyzed zonal changes of longwave and shortwave radiation at the top of the atmosphere with our altered surface albedo (Fig 3). Vegetation-albedo feedback from the inclusion of woody forest over higher latitudes and shrubs and steppes over northern Africa is important in the additional monsoon season rainfall seen for North Africa. Greater vegetation cover for the Sahara and at higher Northern Hemispheric latitudes alters surface albedo by >10% regionally as well as altering absorption of incoming solar radiations across northern hemisphere higher latitudes (Fig 3). Consequently, the pole-equator temperature gradient increases, pulling the ITCZ northwards (see Fig 2). We thus concluded that the control climate generated using PMIP4 vegetation scaled from the mid-Holocene to the 2.5k period provides more precise control conditions to investigate the hydroclimatic impact of volcanic forcing perturbations. Vegetation boundary conditions implemented according to the PMIP4 sensitivity experiments with orbital and greenhouse gas forcing thus helped to produce a precise equilibrium climate for this historically and climatically critical period 2.5ka years ago.

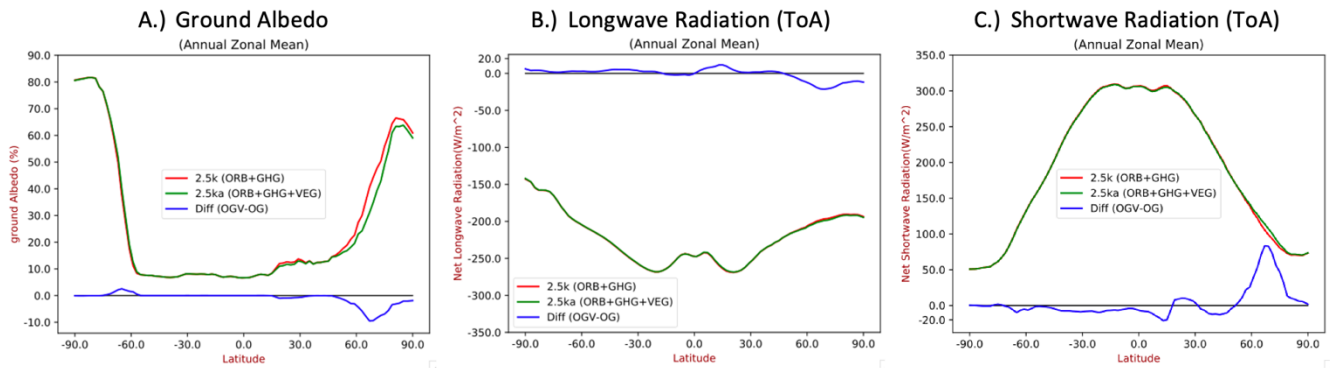


Fig 3. Annual zonal mean of ground albedo (A), longwave & shortwave radiation at the top of the atmosphere (ToA; B and C) for 2.5ka climates with ORB+GHG and ORB+GHG+VEG (red and green lines), respectively. The blue line shows the difference between them. The blue line in panel B & C is exaggerated 10-fold (x10) to show the difference more clearly on the same vertical axis.

3.2. Radiative forcing and climate response to volcanic aerosols

We simulated a series of four eruptions occurring mid-June during the 2nd, 6th, 9th and 12th years of our runs (as per section 2.2 and Table 1). Explosively injected SO₂ oxidizes to form stratospheric sulphate aerosols that can alter the radiative balance at the top of the atmosphere by scattering incoming solar radiation and absorbing and re-emitting longwave radiation. Fig 4 shows the different components of the radiative budget on a monthly scale, with the annual cycle climatology removed for the entire period covering all four eruptions. The relative impacts of scattering shortwave (SW) and absorbing longwave (LW) radiation is proportional to the sulfate aerosol size (Lacis, 1992). The model simulated a lifetime for volcanically injected SO₂ as 31.4±0.72 days for eruption E1 and 24.4±0.44, 25.02±0.40 and 25.5±0.36 days for eruptions E2, E3 and E4, respectively. Other studies have reported a comparable average lifetime of 33 days (Read et al., 1993), 25±5 days (Guo et al., 2004), 35 and 25 days (Bluth et al., 1992; Schnetzler et al., 1995) for SO₂ injected from the 1991 Pinatubo eruption using various satellite retrievals.

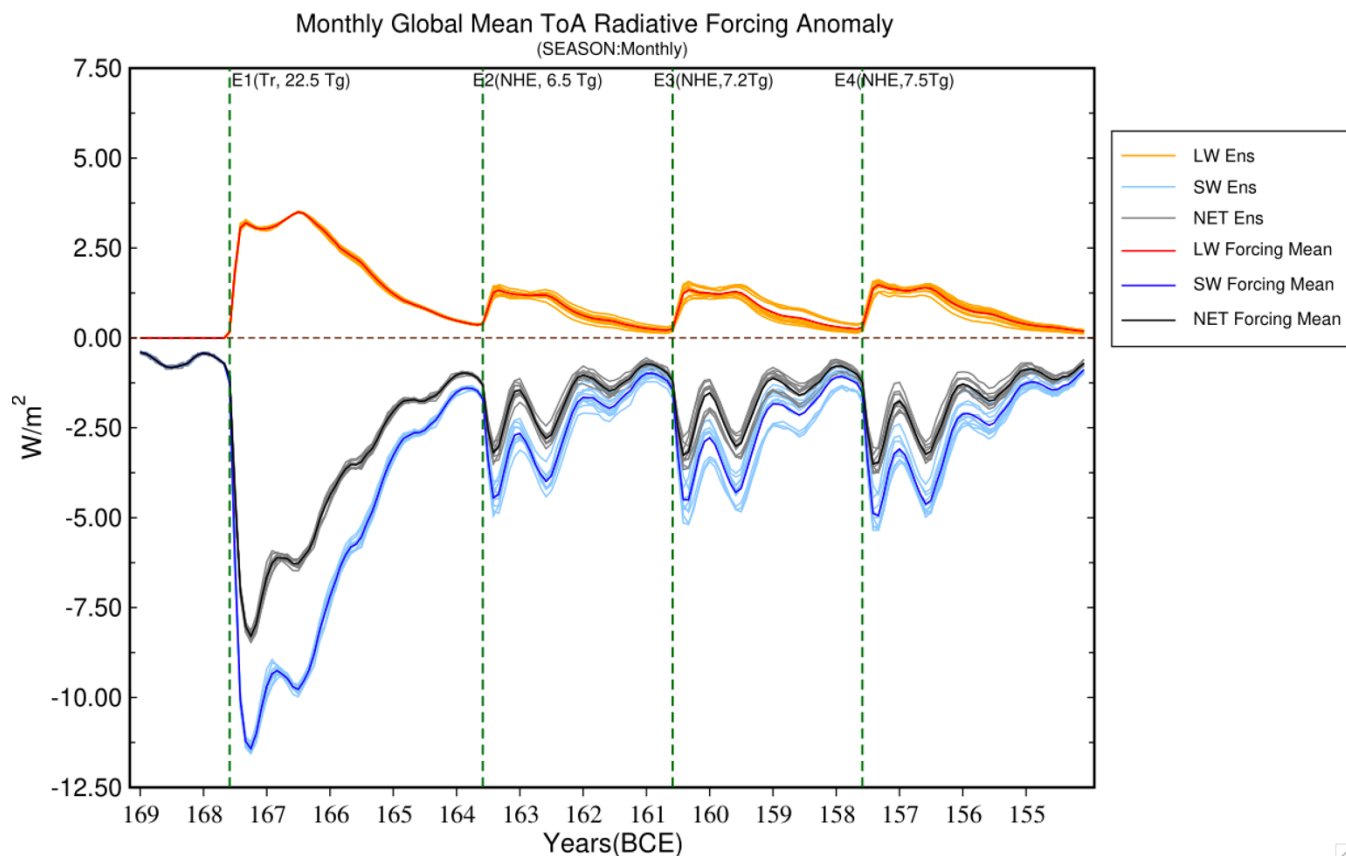


Fig 4: Monthly mean top of the atmosphere radiative balance perturbation due to volcanic aerosols for the entire simulation length. Orange/red shows the longwave radiative response, light/dark blue represents the shortwave, and grey/black represents the net (ToA) radiative change averaged at the global scale. The light-colored solid lines represent individual ensemble members, and the dark-colored lines show the ensemble mean. The green vertical dashed lines show when the eruptions happened.

With 22.5 Tg of SO_2 injected, the first, tropical eruption was larger than Pinatubo ($\sim 30\%$) and altered the longwave radiation budget by a mean of $\sim 3 \text{ W/m}^2$ for almost a year, while the other three eruptions were approximately 1/3rd of Pinatubo and produced a perturbation of the longwave radiative budget by $\sim 1 \text{ W/m}^2$. The model simulated a strong impact on the shortwave radiation budget up to a mean of $\sim 10 \text{ W/m}^2$ for a few months after the first eruption and of $\sim 4 \text{ W/m}^2$ for a few months after each of the subsequent eruptions. A mean imbalance of up to -7.5 W/m^2 after the first eruption and -2.5 to -3 W/m^2 after the other eruptions in the top of atmosphere net radiative forcing suggests a strong corresponding surface cooling.

Note that the bumps in the various radiative forcing trajectories (Fig. 5) in the year after each eruption reflect the northern hemispheric seasonal cycle. The presence of volcanic aerosols in the atmosphere impacted climate in several important ways, described below.

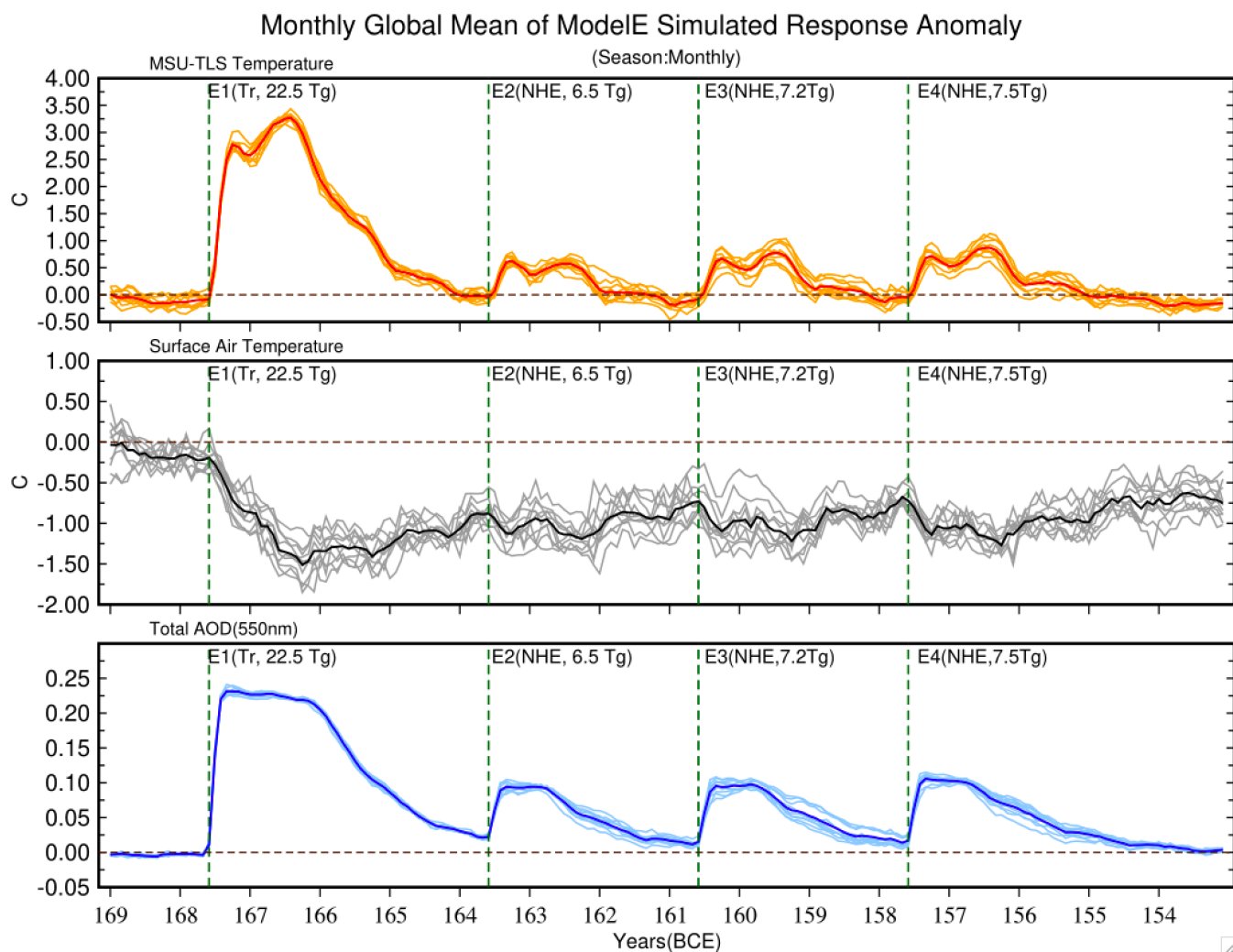


Fig 5. Globally averaged changes in MSU TLS (top panel), surface air temperature (middle panel) and total atmospheric column AOD at 550 nm for each month for the entire simulation period. The light-colored solid lines represent individual ensemble members, and the solid dark colors show the ensemble means. The green vertical dashed lines show when the eruptions happened.

395

400

The top panel in Fig. 5 shows the monthly change in microwave sounding unit (MSU) temperature for the lower stratosphere (TLS) as calculated by the model, which is a typical metric for present-day evaluation of modeled stratospheric temperatures against satellite data. It covers the lower stratosphere, where volcanic aerosols mostly reside, and represents the local atmospheric response of longwave absorption by them. After Pinatubo (1991), a lower stratospheric warming on the order of 2-3°C for a year was estimated using multiple reanalysis products (Labitzke and McCormick, 1992; Fujiwara et al., 2015). This is comparable to the ~25% larger eruption simulated here, E1, in which volcanic aerosols spread over a larger region (in both the northern and southern hemispheres) and absorbed a significant portion of longwave radiation, warming the lower stratosphere by up to 3°C for the first two years post-eruption. This effect intensified during the second year, before steadily declining in Years 3 and 4 with the scavenging of volcanic aerosols. The three subsequent extratropical eruptions warmed the lower stratosphere by up to 0.5° C only, because these were weaker and only affected the northern hemisphere for a shorter period (~18 months).

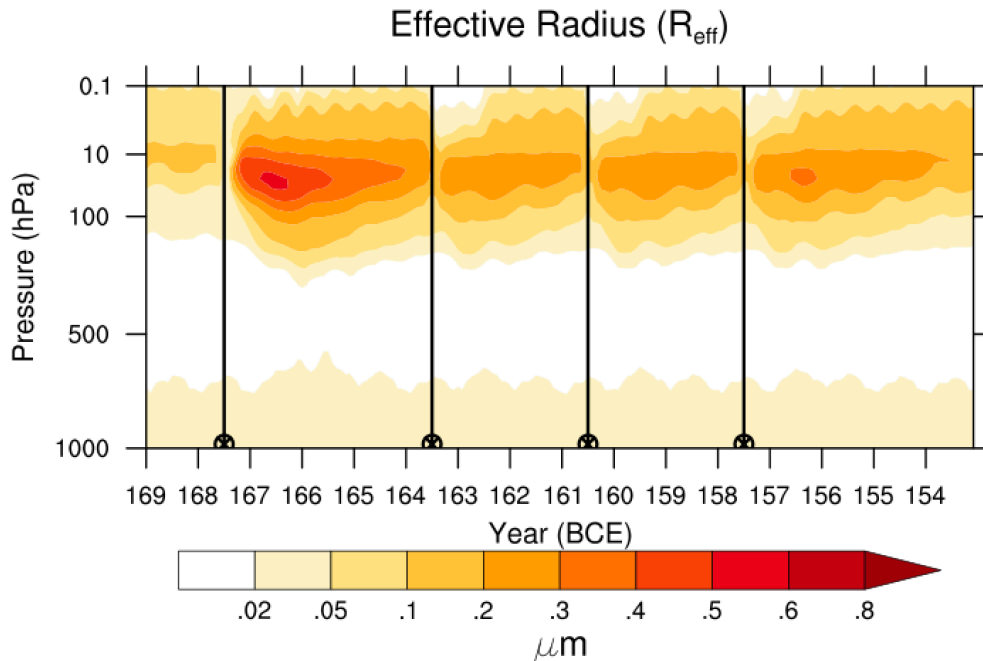
The lower panel in Fig 5 presents the aerosol optical depth (AOD), a measure of atmospheric opacity to incoming radiation calculated as the extinction (sum of scattering and absorption) of shortwave radiation at 550nm. The model simulated an AOD anomaly of around 0.21 for the first 18 months after E1, decreasing as aerosols were progressively removed. The subsequent eruptions produced an AOD of the order of ~0.1 that similarly decreased with time. For comparison, the AOD estimation for Pinatubo (1991) is 0.15 for approximately 12 months over a background optical depth of ~0.6 (Russell et al., 1996; English et al., 2013).

In the upper troposphere and lower stratosphere, the impact of each eruption was distinct with a near-complete recovery to background AOD levels observed after each (i.e., before the next) event; however, at the surface, a lag in recovery time was evident (middle panel, Fig 5). The net impact of radiative flux perturbations following the eruptions is summarized using the global surface air temperature change for the entire period. The model produced a mean cooling of ~1.5° C in the second year after E1 and ~ 1.0° C after all other eruptions. Although AOD recovered a few years after each eruption, the surface temperature response was more prolonged. This lag in response can be mainly ascribed to the thermal inertia of the oceans, requiring a greater recovery time. This is borne out by the sea surface temperature

(SST) response shown in fig S4, with a slower post-eruption recovery and remanent cooling effect. The smaller extratropical eruptions (E2-E4) that followed the large tropical E1 were then observed to hinder surface temperature recovery, maintaining a surface cooling of around 1.0°C for the entire simulation period. Comparatively, Pinatubo (1991) created an ~0.5°C (peak) cooling over 1-2 years post-eruption (Hansen et al., 1996).

3.3 Volcanic aerosol properties

Radiative forcing from volcanic aerosols is tightly controlled by aerosol size (Lacis et al., 1992; Hansen et al., 1980). The aerosol effective radius, R_{eff} , is a key metric in linking aerosol microphysical properties with their SW and LW impacts. The vertical profile of aerosol size as represented by R_{eff} was calculated for each month (Fig 6). After the tropical eruption (E1), new aerosols nucleated and grew rapidly via coagulation and, while SO₂ was still available, by condensation, and attained a maximum R_{eff} of >0.5 μm approximately for 2 years. In comparison, R_{eff} after Pinatubo (1991) increased to 0.6 μm and sustained that size for approximately 2 years (Russell et al., 1996). Sulfate aerosol sizes for the three subsequent extratropical eruptions (E2 to E4) grew up to 0.3 μm.



445 Fig 6. Timeseries of global ensemble mean vertical profile of sulfate aerosol R_{eff} for the entire simulation period. The vertical black line with a circled cross mark on the horizontal axis shows the eruption timings.

The aerosol extinction vertical profile (Fig S5A) shows that the radiative impact of the E1 tropical eruption in the lower stratosphere was prolonged as compared to the later extratropical eruptions. Lower
450 stratospheric heating affects the dynamics of the stratosphere; after tropical eruptions enhanced tropical upwelling and extratropical downwelling with the phase of Brewer-Dobson circulation impact upon the transportation of trace species such as Ozone (O_3) and NO_2 (Aquila et al., 2013; Trepte et al., 1992; Pitari et al., 2016; Pitari and Mancini, 2002). Fig S5B shows a strong positive (≥ 10 ppbv) anomaly of CH_4 in the upper stratosphere and negative (≤ 10 ppbv) anomalies in the lower stratosphere, especially after the
455 tropical eruption (E1). Changes in the mean concentration of upper and lower stratospheric methane (CH_4) suggest a strong vertical transport (Kilian et al., 2020).

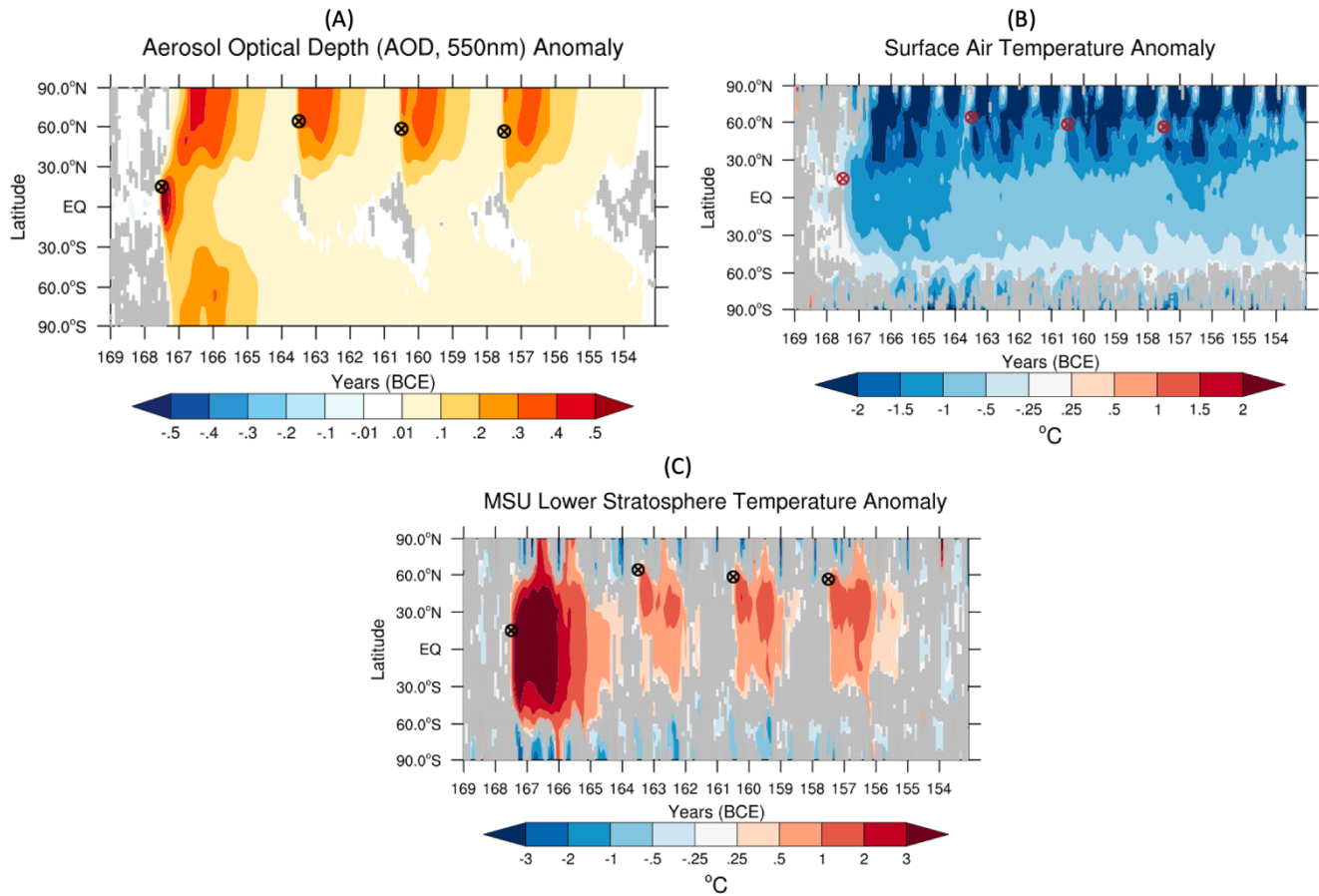
3.4. Latitudinal temperature response to volcanic aerosol forcing

The Hovmöller diagram (Fig 7A, 7B) shows the differences between the zonally averaged AOD at 550nm
460 and surface air temperature response for the ensemble means of the volcanic eruption simulations compared to the mean climatology of the control simulation. The statistical significance level is estimated using the 2-tail student t-test after Deser et al. (2012) and following the assertion that 10 ensembles are sufficient for reasonable estimation of internal variability at a regional scale (Singh and AchutaRao, 2019). The pattern of total AOD after the first eruption (E1) showed a strong cross-equatorial transport
465 of stratospheric aerosols into the southern hemisphere, with a similar pattern in the northern hemisphere. This is consistent with the hypothesis that an enhanced Brewer-Dobson circulation in the southern hemisphere during the austral winter can lead to the southward transportation of volcanic aerosols after a Pinatubo type (tropical) eruption (Aquila et al., 2012). The initial dispersal of aerosols from eruption E1 was strongly influenced by its timing and exhibited a seasonal dependence (consistent with Toohey et al.,
470 2011). However, the other three eruptions (E2, E3 and E4) in the high latitude Northern Hemisphere only yielded an increased AOD in that hemisphere.

A lag of more than 12 months in peak surface temperature response (Fig 5, Middle panel) after E1 correlates well with the modelled aerosol distribution, consistent with reporting for similar events (e.g.,

Jungclaus et al., 2010; Klocke, 2011). The peak global mean surface temperature response thus appeared
475 when aerosols from the tropical eruption (E1) had extended across the northern hemisphere extratropics
and polar regions. It should be noted that northern extratropical land surfaces responded quickly to the
attenuated post-eruption shortwave radiative flux compared to the tropics. The zonally averaged surface
temperature response (fig 7B) showed that a strong cooling of 1.0-1.5°C lasted over the tropical north and
partially over the tropical southern hemisphere for more than 30 months after E1. Further, the largest
480 anomalies of >2.0 °C cooling mostly appeared six months after E1, with the subsequent extratropical
eruptions helping to maintain the northern hemispheric cooling.

The seasonality of surface temperature response revealed a more substantial cooling during the boreal
summer season for all four eruptions and for E1 also revealed the expected post-tropical-eruption winter
warming pattern over Europe. Fig S6 shows the spatial pattern of the surface temperature response to
485 volcanic aerosols over the four seasons directly following E1 (JJA & SON for the eruption year and DJF
& MAM for first year following). The response for the first two seasons was confined to the tropics but
moved to higher latitudes thereafter. As evident in fig S3, the winter (DJF) post-eruption warming over
Europe and an observed cooling over Northern America may result from the same fundamental
atmospheric dynamics noticed after Pinatubo (1991) (Robock, 2000; Robock and Mao, 1992).



490

Fig 7. Hovmöller diagram showing the zonally averaged temporal dispersion of volcanic aerosols in terms of AOD change at 550nm (A), surface temperature response (B), and lower stratospheric temperature response (C). Anomalies were calculated with respect to a climatological annual cycle calculated from the control simulation. The gray color is painted over regions where changes are not statistically significant at the 95% confidence level. Circled cross marks show the modeled spatial and temporal position of the eruptions.

495

The global lower stratospheric temperature response in terms of MSU TLS data was discussed in section 3.2. Interestingly, fig 7C shows that the latitudinal anomaly of the lower stratosphere warming was broadly limited to the equatorial lower stratosphere. E1 induced lower stratosphere warming on the order of >3 °C, with a weaker warming of up to 1-2 °C after E2, E3 and E4. Lower stratosphere warming is also known to affect the polar vortex strength in the northern hemisphere and atmospheric circulations

500

into the troposphere, with repercussions for surface climate and variability patterns (e.g., Graf et al., 1993, 2007; Shindell et al., 2004).

505

3.5 Latitudinal precipitation response to volcanic aerosols

We used a coarser resolution earth system model having a simplified parameterization and successful in simulating the large-scale patterns of rainfall change (Kelley et al., 2020). Studies of observational records plus modeling efforts have demonstrated that the cascading impact of an altered radiative balance at the top of the atmosphere due to volcanic eruptions is reflected in the hydrological cycle in regional patterns of seasonal rainfall change (e.g., Robock and Liu, 1994; Robock, 2000; Trenberth & Dai, 2006; Schneider et al., 2009, Iles et al., 2012; Iles and Hegerl, 2014; Timmreck, 2012). We investigated the hydrological cycle response to the 168-158 BCE eruption quartet at both a global and regional scale, paying particular attention to the northern hemispherical monsoon season (JJAS) for the first 2 years following each eruption. Any individual ensemble member might best represent the historical reality, but it is impossible to select the most accurate member absent supporting observational data from the period. Also, added noise due to natural variability can be greater at the regional scale, even to the extent of altering the sign of observed changes among the individual ensemble runs. Thus, we mainly focused upon the mean from across the ensemble when examining the response to the eruptions for the various climate variables considered. Fig 8 shows the Hovmöller diagram of the zonal mean precipitation anomaly relative to the annual cycle climatology of the 100-year-long control simulation.

510
515
520

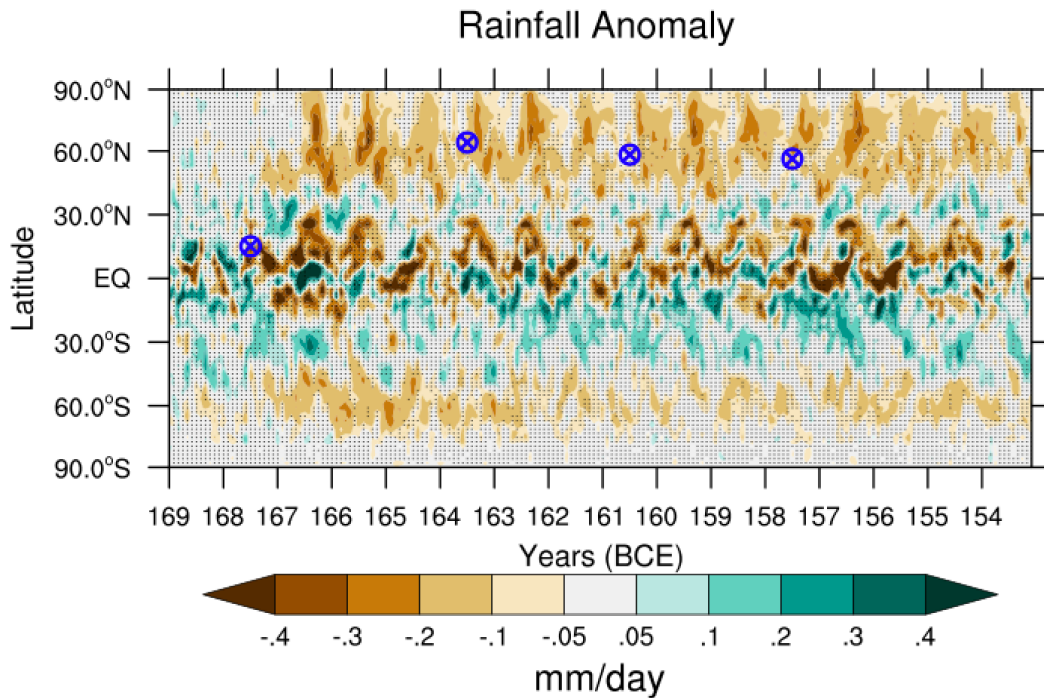
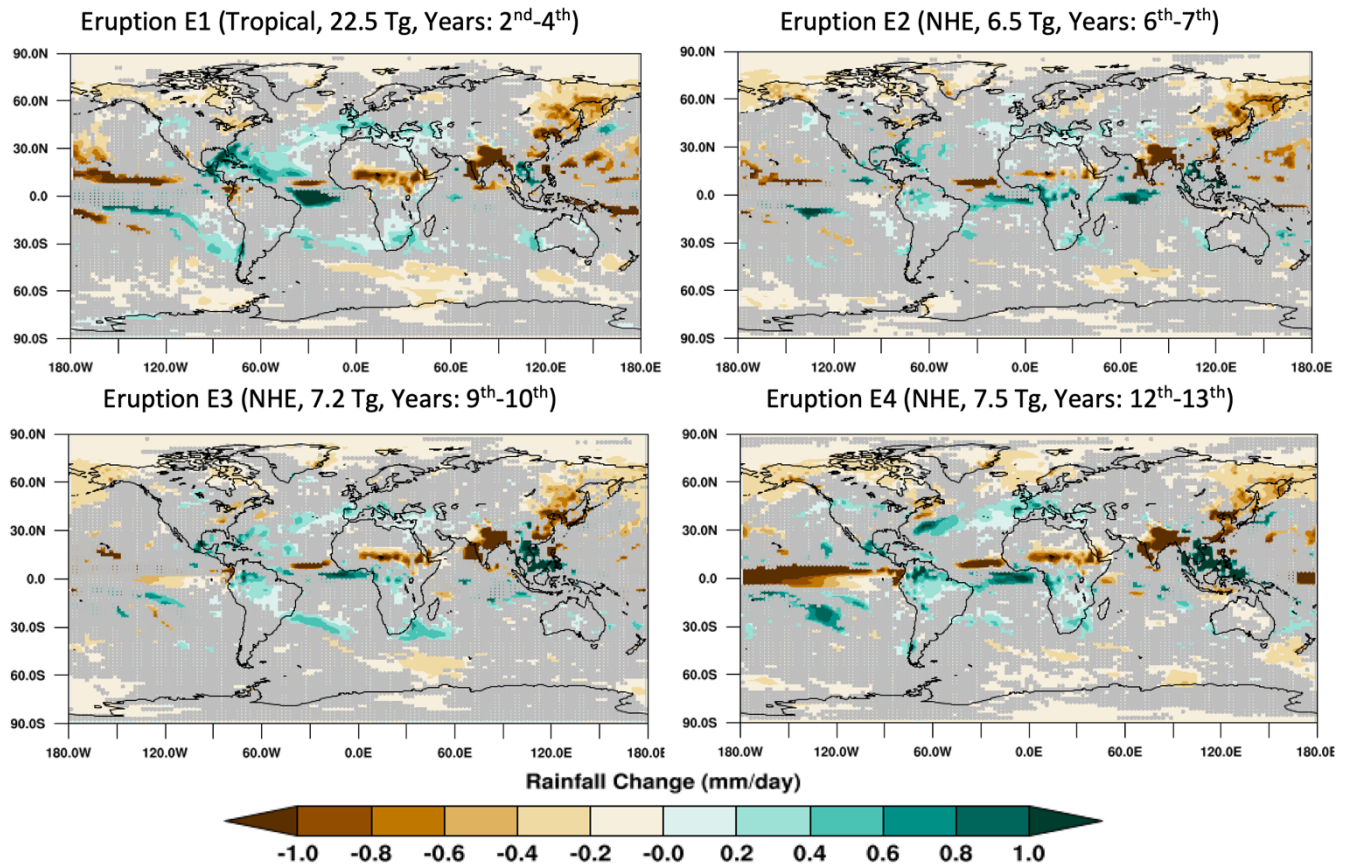


Fig 8. Hovmöller diagram showing the zonally averaged rainfall anomaly for the entire period as the
 525 spatiotemporal response of global rainfall to our series of volcanic eruptions. Circled cross marks show
 the locations and timing of the eruptions. Black dots point out regions where changes are not statistically
 significant at the 95% confidence level.

The ensemble zonal mean post-eruption rainfall change showed a substantial negative trend in the
 530 northern hemisphere due to the volcanic aerosol-induced cooling. A robust negative anomaly on the order
 of 0.3-0.4 mm/day in the northern hemisphere rain belt (ITCZ) region appeared shortly following E1 and
 persisting for several years (Fig 8). A pattern of strong drying in the equator also coincided with the
 northern hemisphere monsoon season (JJAS) for 2 to 3 years after E1. However, because the northern
 hemispheric extratropical rainfall response strongly correlates with the surface temperature response, it
 535 thus emerged here 12 months after E1, with the model calculating a moderate to high decrease on the
 order of 0.1-0.2 mm/day, persisting throughout the year for three post eruption years. A shift in the
 northern hemisphere rainfall pattern was also evident for the region around 30°N, with slight increases in
 rainfall for 2 years after E1. This response was statistically significant over only a few spots, however.
 Fig 8 demonstrates that a drying pattern also prevailed after the later extratropical eruptions (E2-E4).

540 Thus, the northern hemisphere experienced a sustained net (albeit temporally varying) precipitation decline for the entire modeled period, with a distinct seasonal character.



545 Fig 9. Mean change (mm/day) in northern hemisphere monsoon season (JJAS) rainfall averaged for three consecutive years after eruption E1 (including the eruption year) and two years each after E2, E3 and E4 (including the eruption years) (left to right and top to bottom). The caption over each panel shows the eruption characteristics. A gray color is painted over the grid boxes for which rainfall change is not significant at the 95% confidence level. Years indicated in parentheses follow the order of the eruptions
550 in our simulation period, i.e., E1 occurs in the 2nd simulation year, and E2-E4 occur in the 6th, 9th and 12th years, respectively.

We further evaluated the spatial patterns of change in mean rainfall during the northern hemisphere monsoon season (JJAS) (fig 9). We averaged the three monsoon seasons (eruption year and next 2 years)
555 after the more potent tropical eruption (E1) and two monsoon seasons (eruption year and next year) after

each of the extratropical eruptions (E2, E3 and E4), focusing principally on statistically significant responses. After E1, summer monsoon rainfall appeared strongly suppressed over many major northern hemisphere monsoon regions. Importantly for our focus on Egypt, African monsoon rainfall showed a notable decrease of 0.5-1.0 mm/day during the three-year post-eruption JJAS season average (i.e., derived from the eruption year and first two post-eruption years). This decrease covered a large area in Africa from (approximately) the equator to (approximately) 17°N. The South and East Asian monsoon regions also exhibited a robust negative rainfall anomaly of >1.0 mm/day over the Indian subcontinent and (more variably) several regions of China, though with some isolated increase over the eastern Vietnamese landmass. Similar patterns of decrease appeared over the western (particularly northwestern) Pacific and northern hemispheric high latitude regions more broadly. The model also simulated a (statistically significant) band of enhanced JJAS rainfall stretching from Central Asia westward through the Middle East and into the Mediterranean (touching parts of northern Africa), Western European and parts of the North Atlantic (roughly between a latitudinal band of 30°N to 50°N). A contiguous band of increased rainfall was observed further south and west in the Atlantic, stretching into parts of the northern Caribbean, southeastern Gulf of Mexico and Mesoamerica (fig 9).

Similar patterns of suppressed boreal monsoon season rainfall were observed following the extratropical eruptions (E2-E4), but a particularly notable east-west band over land and ocean (broadly confined between slightly north of the equator and 30°S) shows a positive rainfall anomaly (most clearly statistically significant between (approximately) 5°N and 10°S (fig 9)). This is largely consistent with observations and modeling of volcanic climatic impacts under a range of scenarios and periods (e.g., Robock, 2000; Robock and Liu, 1994; Iles et al., 2012; Liu et al., 2016; Haywood et al., 2013; Schneider et al., 2009; Trenberth and Dai, 2007; Joseph and Zeng, 2011; Gu and Adler, 2011). Of mechanisms, for many northern hemisphere landmasses, these eruptions induced a surface cooling that altered the meridional (equator-to-pole) surface temperature gradient (fig 7). Given this energetic deficit, we posit that the northern hemisphere experienced a post-eruption alteration of large-scale circulation patterns and moisture convergence, producing a constrained northward ITCZ migration during the boreal summer, diminishing rainfall over many northern hemispheric monsoon regions and (relatedly) promoting increased rainfall in the above-described band from the equator southward (Liu et al., 2016; Oman et al.,

2006; Graf, 1992; Dogar, 2018). This is consistent with Colose et al. (2016), They demonstrated that a hemispherically asymmetric volcanic forcing creates energetically deficient conditions in the hemisphere of the greatest forcing that “pushes” the ITCZ away from it. Palaeoclimatic data also shows that tropical and northern hemispheric eruptions can create a dipole resulting in wetter summer conditions over extensive parts of the Mediterranean, with correspondingly drier conditions over northern Europe (Rao et al., 2017). This is also largely consistent with our model output (fig 9).

590

3.6 African monsoon and Nile River response

Our modeling suggests that all four eruptions, 168-158 BCE, are likely to have influenced rainfall over different monsoon regions in the northern hemisphere for 2-3 years after each eruption, in combination producing a sustained deficit for more than a decade. Focusing on the North African monsoon region, fig 10 shows three consecutive years of JJAS rainfall over equatorial and northern Africa (encompassing the Nile basin) after each eruption. The African monsoon exhibited notably reduced rainfall of >1 mm/day following the (mid-June) E1 tropical eruption, starting in the eruption year itself (Year 0, fig 10), affecting both the White Nile watershed in the south of the basin and the Blue Nile and Atbara River watersheds further north and east in the Ethiopian Highlands. Reduced precipitation was also observed following each (also mid-June) extratropical eruption (E2-E4) during the eruption years but was more spatially constrained (and particularly for E2, less severe). This is perhaps unsurprising as the estimated SO₂ output of E2-E4 is approximately 1/3 of E1. Nonetheless, in each case the Blue Nile and Atbara River headwaters experienced a statistically significant decrease, with implications for the summer flood in Egypt, which depends for approximately 80% of its floodwater on rainfall there (Melesse et al., 2011). For E2-E4, this response intensified in the first full post-eruption year (Year 1, fig 10), persisting into the second full post-eruption year (Year 2, fig 10), while for E1 the response contracted geographically in Years 1-2, resembling that seen after E2-E4 (fig 9, fig 10). This suppression of the African monsoon following tropical and northern hemispheric extratropical eruptions is consistent with previous studies (e.g., Colose et al., 2016; Oman et al., 2006; Haywood et al., 2013; Jacobson et al., 2020; Manning et al., 2017).

610

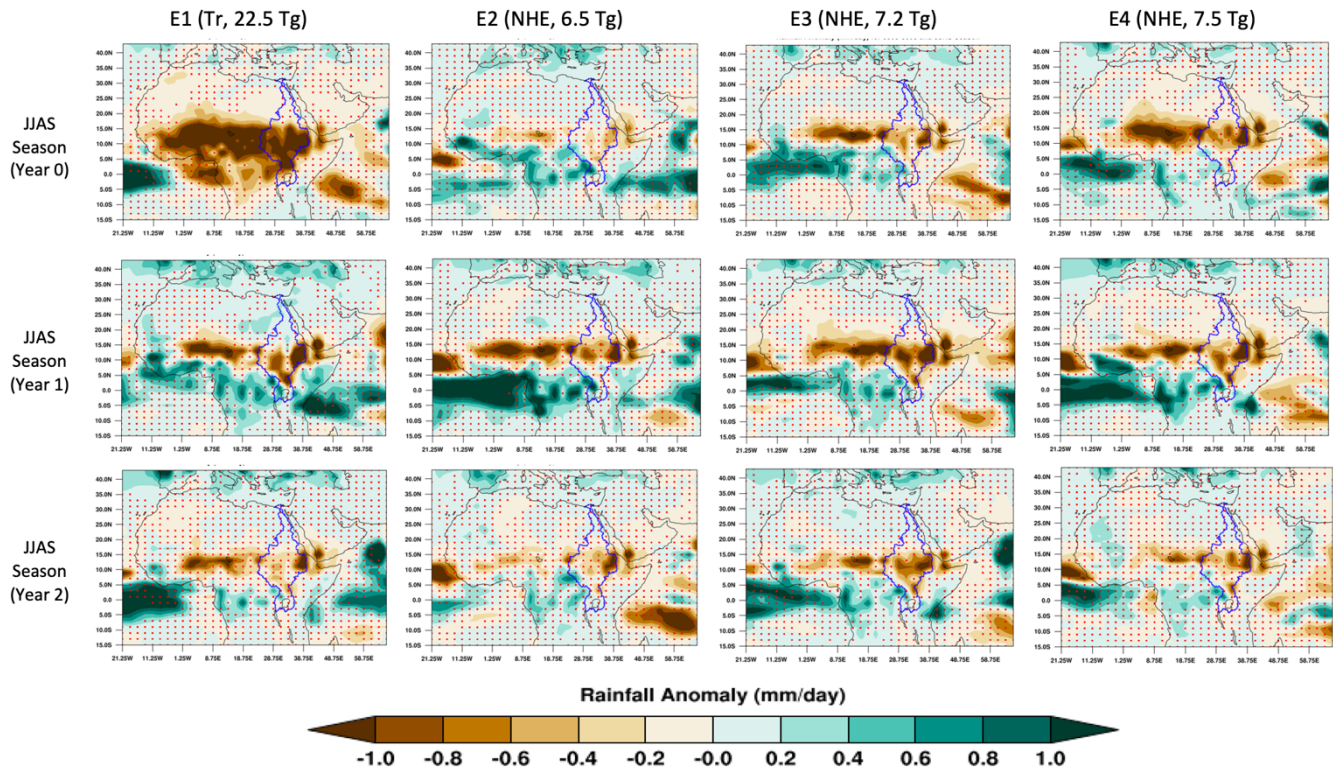


Fig 10. Ensemble mean rainfall difference from the climatological control for each of the first three monsoon seasons (JJAS; rows) after each eruption (columns) over equatorial and North Africa. The blue boundary line shows the present-day Nile River basin, broadly similar to the river extent approximately 2.5ka years ago. The red stippling indicates regions over which change in rainfall is not statistically significant at a 95% confidence level.

Spatial patterns in total cloud cover (fig S7) for the three consecutive post-eruption monsoon seasons showed a decrease of up to 10% over East Africa and the adjacent Indian Ocean region. This is consistent with the above-reported negative rainfall anomalies (>1 mm/day) over North African land regions, especially over the watershed of the Nile River basin, again suggesting a notable weakening of the summer monsoon (Graf, 1992, Oman et al., 2005). Positive total cloud cover anomalies also coincided with regions having a positive rainfall response (e.g., Mediterranean, Middle East).

We also analyzed the mass of total annual water flow averaged over the Nile River basin (blue line, fig 11) as representative of Nile flooding and discharge at the river's mouth to summarize the volcanic impacts on Nile flooding. Table 2 presents the percentage annual deficit (-) or excess (+) of water flow in

the Nile River basin after each eruption along with the variability (one standard deviation) observed across the model ensemble members, relative to the 100 years climatological mean (base climate). E1 had a strong impact (>30% deficit) on water mass over the Nile catchment during the eruption year and first full post-eruption year (Years 0 and 1, table 2), with a more moderate decrease of ~13% during the second full post-eruption year (Year 2, table 2). The first extratropical eruption (E1) showed a minor decrease in the eruption year (Year 0, table 2) that was not statistically significant. The following two full post-eruption years reversed this pattern to exhibit a modest (though not statistically significant) increase. Extratropical eruptions E3 and E4 showed a more consistent decrease. This was on the order of ~ -5% in the eruption year (Year 0, table 2) for both, becoming notably greater in the first full post-eruption year (Year 1, table 2), being ~ -18% for E3 and ~ -12% for E4. This decrease persisted into the second full post-eruption year (Year 2, table 2) for E4 (~ -12%), but fell back in line with the 100 years climatological mean for E3 (though this mean exhibited the highest variance among ensemble members (table 2)). Several individual ensemble members have simulated the change in river flow at the 95% confidence levels ($1.95 \cdot \sigma_{\text{ctrl}}$; σ denotes standard deviation) for a few years when compared against the variability for the control period.

Table 2. Annual mean change (%) and standard deviation in water mass flow over the Nile River catchment for 3 consecutive years after each eruption. Control run variability (interannual standard deviation about the decadal mean, σ_{ctrl}) for Nile basin river flow is 25.2%.

	E1(Tr, 22.5 Tg) Change /Std	E2(NHE, 6.5 Tg) Change /Std	E3(NHE, 7.2 Tg) Change /Std	E4(NHE, 7.5 Tg) Change /Std
Year 0 (eruption year, mid-June)	-28.7±39.9	-3.02±22.5	-4.9±35.2	-4.7±29.6
Year 1	-37.8±22.5	2.5±36.7	-18.1±28.9	-11.7±29.9
Year 2	-13.4±32.2	10.7±39.9	0.9±47.8	-12.1±28.0

The spatial patterning of response across a basin as complex as the Nile is a critical consideration (fig 11). After E1, the above-described rainfall suppression is associated with a drastic reduction in annual river flow observed over effectively the entire river basin, with a simulated decrease of approximately 30, 40 and 15 km³ relative to the 100 years climatological mean (~104 km³) for Years 0 to 2, respectively. After E2, total annual river flow in Year 0 slightly increased (table 2), although this response was not statistically significant, and in Year 1 exhibited a marked contrast between (particularly) the southern (greater flow) and northern (lesser flow) parts of the basin, before a more consistent increased flow was observed in Year 2. The contrast between a reduced flow over (broadly) the northern part of the basin versus increased flow over the southern part was then observed consistently for all post eruption years for E3 and E4 (fig 11). This contrast may arise in part as a function of the size and complexity of the Nile basin (and the markedly different geographical location of rainfall supplying the White Nile to the south and Blue Nile and Atbara River to the northeast), combined with the asymmetrical (northern hemispherically biased) aerosol loading after extratropical eruptions, suppressing the northward boreal summer migration of the ITCZ and associated rain-bearing monsoon winds (as discussed earlier). As these winds are the primary driver of summer rainfall over the Ethiopian highlands, summer flooding of the Blue Nile and Atbara River into the north of the basin and Egypt would be diminished, while water flow down the White Nile (fed by rainfall over the equatorial lakes) would be potentially enhanced by the failure of the ITCZ to migrate northward beyond this region.

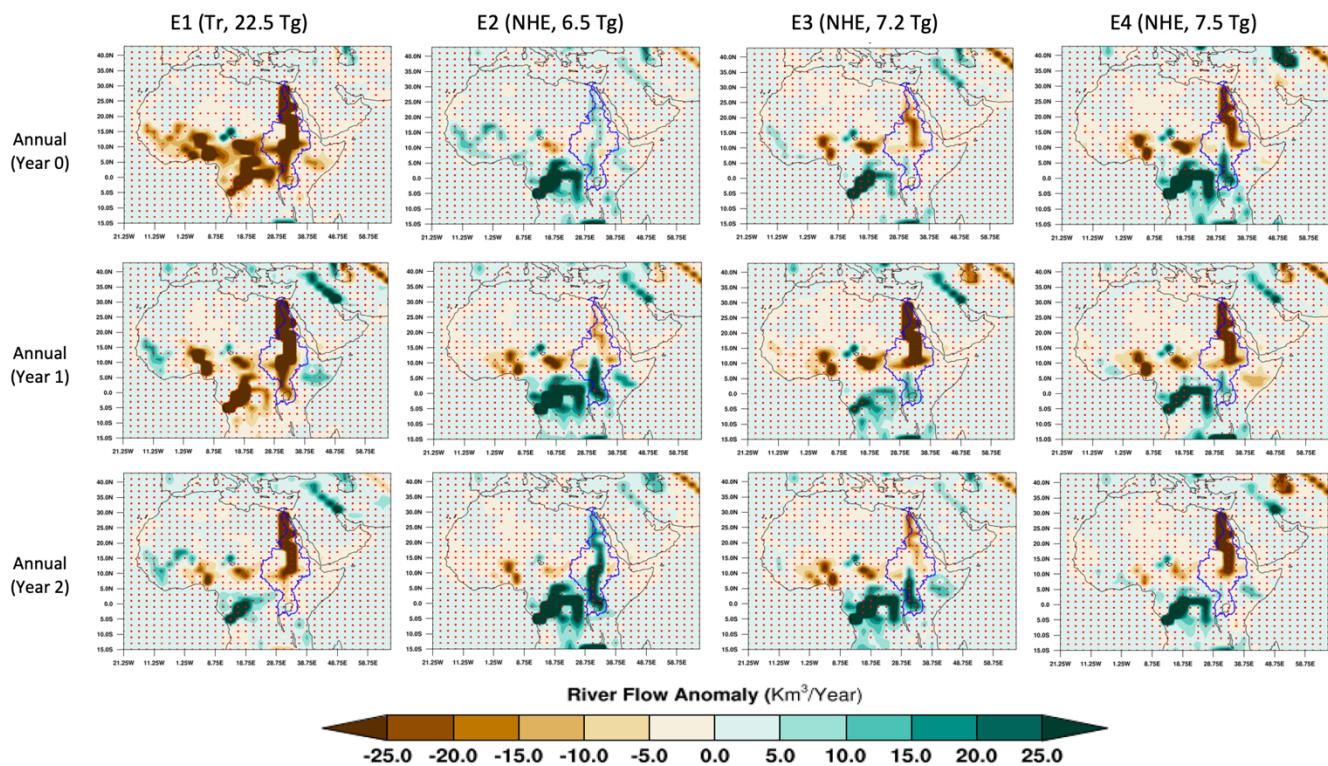


Fig 11. Annual river flow anomaly (km^3/year) relative to the control climatology for 3 consecutive years after each eruption (columns) over North Africa. Other details as per fig 10.

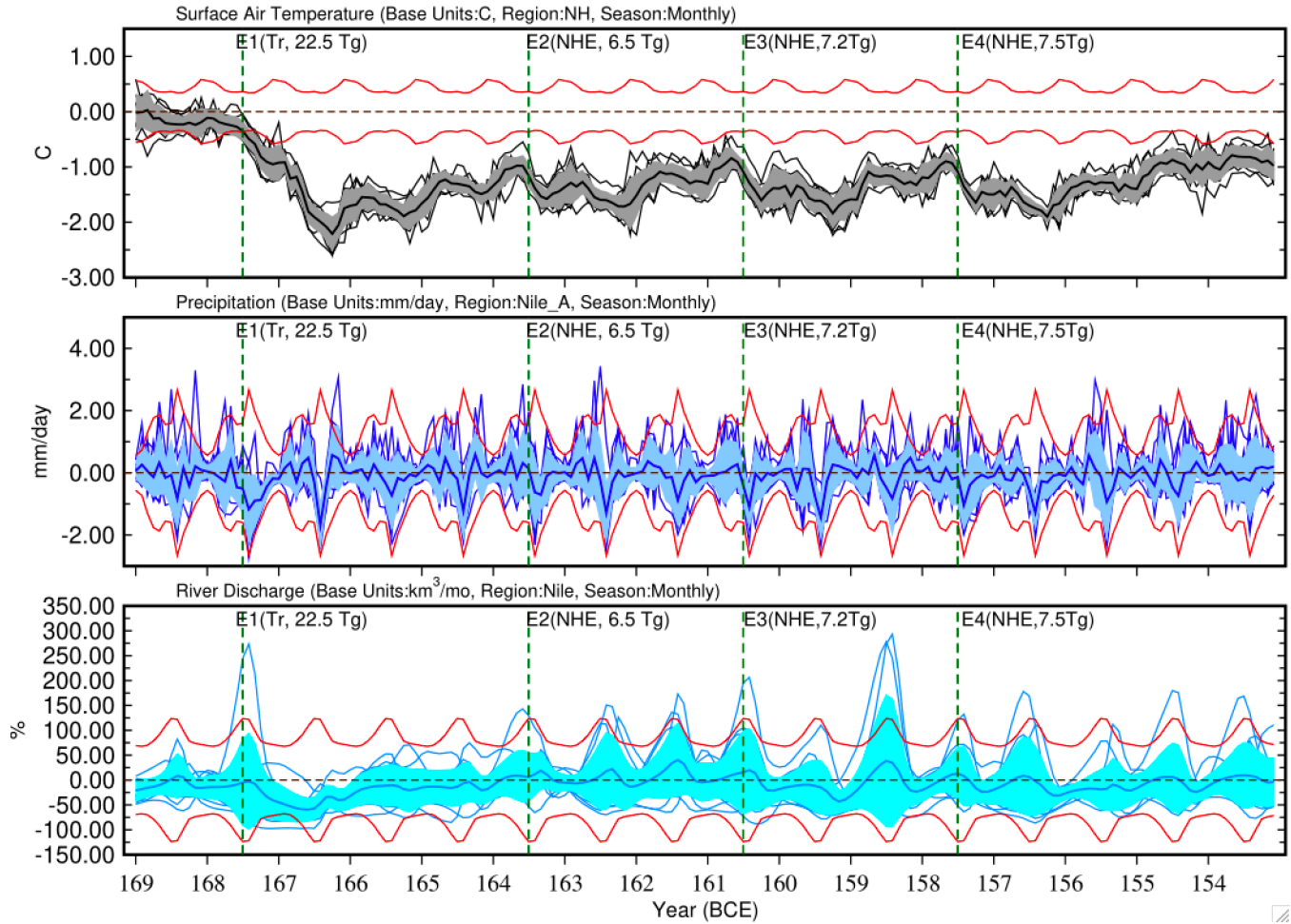
670

To summarize the hydroclimatic impact of this volcanic quartet on the Nile River basin, fig 12 (top panel) shows that the northern hemisphere experienced a substantial cooling of $\sim 2.5^\circ\text{C}$ (1.0°C greater than the global average response) with a lower spread among ensembles after the first eruption (E1). The subsequent eruptions (E2, E3, and E4), reoccurring at equal temporal intervals, maintained a cooling of $\sim 1.75^\circ\text{C}$ for at least a decade. The monthly mean rainfall anomaly over the Nile basin was observed as a considerable decrease varying between ~ 1.0 and 1.5 mm/day during the monsoon seasons (JJAS) for each post-eruption year (fig 12, middle panel). The impact of decreased rainfall over this region is strongly evident after the tropical eruption E1 in discharge at the Nile mouth (grid box centered at 29.0N , 31.25E) in the Nile delta region of Egypt (fig 12, bottom panel). Our modelling showed here a mean deficit beginning in the eruption year (Year 0) and peaking at a reduction of more than 50% during the first full post-eruption year (Year 1), effectively requiring 2 further years to recover. There was no persistent negative discharge anomaly evident after E2, although individual ensemble variability around the mean

680

is quite high. By contrast, a deficit began in the year of E3 (Year 0) that persisted throughout the first full post-eruption year (Year 1) and into the start of the second full post-eruption year (Year 2). This deficit peaked in Year 2 at just less than 50%. A similar response was observed after E4, with a persistent negative anomaly starting in the first full post-eruption year (Year 1), continuing throughout Year 2 and into the start of Year 3. This deficit also peaked in Year 1 (at approximately 30%).

Spatially Averaged Anomaly for ModelE diagnostics



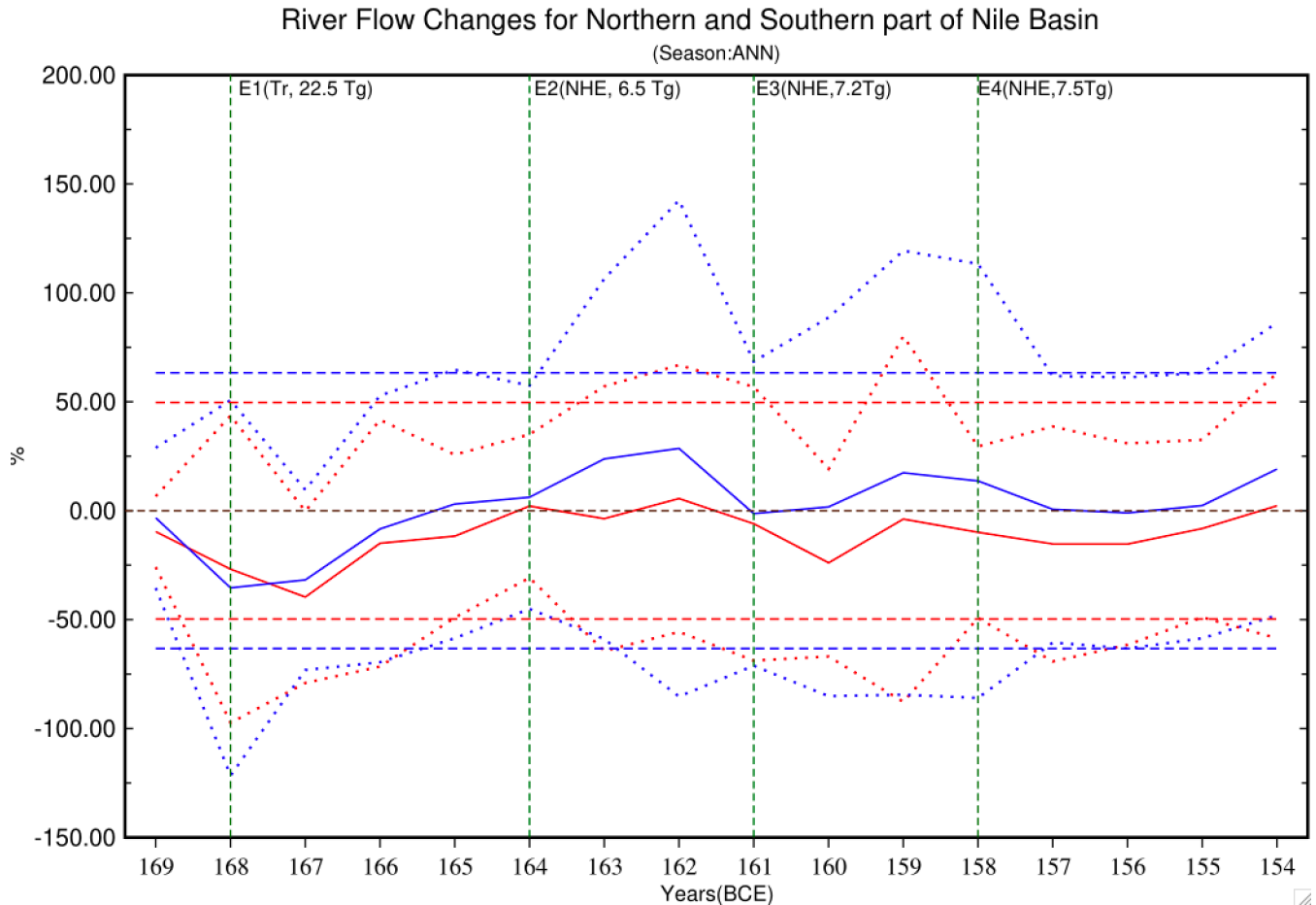
690 Fig 12: Monthly time series of individual ensemble and mean of surface temperature response ($^{\circ}\text{C}$) averaged over northern hemisphere (NH) (top panel), rainfall change (mm/day) for the model's spatial box representing the Nile River watershed (Latitude: (5N, 18N), Longitude: (30E, 42E)) (middle panel) and Nile River discharge anomaly (%) at the delta region (grid box centered at 29.0N, 31.25E). For each panel, the darker solid (thick) line shows the multi-ensemble mean, individual member (thin line), and

695 the color envelope shows the associated variability ($\pm\sigma$; Standard deviation). The annual cycle of climate variability of the control run is shown as $2\sigma_{\text{ctrl}}$ lines (red solid line) along the x-axis for all three variables. The vertical dotted green line shows when each eruption happened.

It is evident that the mean surface temperature response in the northern hemisphere is significant at the control period's $2\sigma_{\text{ctrl}}$ level (95% significance). However, while rainfall and river discharge responses are not significant at the $2\sigma_{\text{ctrl}}$ levels, several individual members do show significance at $2\sigma_{\text{ctrl}}$ as well. This signifies the important influence of the model's internal variability in representing the regional hydrological response to volcanic eruptions. However, the statistical significance of the rainfall and discharge response may be sensitive to the relatively coarse resolution of the GISS ModelE, as well as the boundaries chosen to model the Nile basin and its headwaters. We thus investigated the post-volcanic change in river flow for the southern (White Nile-dominated) and northern (Blue Nile and Atbara river-dominated) parts of the basin by dividing it at 10° N (Fig 13). Annual mean river flow change for the south (blue lines) and north (red lines) of the Nile basin were in broad agreement with a negative flow anomaly after eruption E1. This was most notable in the eruption year and the first year following, with the 95th percentile envelopes (dotted lines) deemed significant at the 95% confidence level for both these years (i.e., crossing the dashed lines parallel to the x-axis (fig 13)). In contrast, the mean north and south responses disagreed, including in the sign of the observed changes, after the extratropical eruptions (E2, E3 & E4). More specifically, while the mean flow anomalies in the year of E2 were unremarkable, with little north-south contrast, a more notable divergence was observed in the first full year following, with a positive flow anomaly in the south and negative in the north. In the year of E3, flow in the south showed no notable anomaly, while flow in the north was marginally negative. This distinction became more marked in the first full year following, mainly due to a larger negative anomaly in the north. In the year of E4, a negative anomaly was again observed in the north, persisting for three post-eruption years, and contrasting with positive or unremarkable anomalies in the south.

720 These results are consistent with our earlier-described results (e.g., spatial rainfall variability over the Nile River basin, as per figs 10 and 11) and proposed mechanisms, alongside expectations from the literature (e.g., Manning et al., 2017). Thus, tropical eruptions (like E1) may produce a more consistent (negative) north-south flow response due to their more even interhemispheric aerosol burden and

725 associated radiative impact. Extratropical NH eruptions (like E2-E4) that can result in a more asymmetric hemispheric aerosol burden may, by contrast, introduce contrasting flow anomalies by suppressing the northward migration of the ITCZ, negatively impacting flow in the Blue Nile and Atbara rivers by diminishing monsoon rainfall in the Ethiopian highlands, while potentially enhancing flow in the White Nile, fed by rainfall over the equatorial lakes.



730 Fig 13. Annual Nile River flow changes averaged over the northern (red) and southern (blue) parts of the basin (divided at 10° N) for the entire simulation period. The solid lines represent the ensemble mean for each part of the basin; the dotted lines are $\pm 1.95\sigma$, where σ is derived from across all the ensembles, and the horizontal dashed lines parallel to x-axis are the $\pm 1.95\sigma_{ctrl}$ where σ_{ctrl} is the standard deviation across the 100-year control run. Red and blue lines correspond to the northern and southern parts of the Nile
 735 basin, respectively.

4. Discussion and Conclusions

Recent years have seen increasing interest in the role of hydroclimatic variability in human history, including by interdisciplinary teams combining evidence and methods across disciplinary divides (e.g., McCormick, 2011, 2019; Manning et al., 2017; Ludlow and Travis, 2019; van Bavel et al., 2019; Degroot et al., 2021; Ljungqvist et al., 2021; Travis et al., 2022; Izdebski et al., 2023). For the pre-modern era, when systematic observations of hydroclimate become scarce, this effort depends increasingly upon natural archives (palaeoclimatic proxies) that track variability at spatial and temporal resolutions sufficiently high to convincingly identify associations with societal phenomena (e.g., subsistence crises, migration, conflict), economic and demographic processes, and major historical events (e.g., “collapse” of empires). Work such as that by PAGES2k Network members offering paleoclimatic reconstructions and data collections (e.g., PAGES 2k Consortium, 2013; PAGES 2k Consortium, 2017) are thus crucial, although here the exclusive focus on the past 2k years (for some proxies an artificial horizon and for others an aspiration), excludes many foundational periods and events in human civilization. This includes the development of advanced ancient societies in Asia, the Near East and Mediterranean that are richly documented and offer considerable potential for the study of socioecological systems.

Important work has still been possible using speleothems, sedimentary and other archives (e.g., Drake, 2012; Schneider and Adali, 2014; Knapp and Manning, 2016; Sołtyśiak, 2016), but there is often little direct temporal and/or geographical overlap between these early ancient world regions of rich human documentation and proxies (e.g., tree-ring based) with precision and accuracy at annual-or-better resolutions. A major advance has been the publication of a chronologically precise and accurate bipolar ice-core-based volcanic forcing reconstruction for the past 2,500 years (Sigl et al., 2015; Toohey and Sigl, 2017). The potentially global hydroclimatic impacts of major explosive eruptions makes this record widely geographically relevant, while the repeated incidence of major eruptions that can be identified through sulphate deposition in the polar ice sheets has allowed their use as “tests” of societal vulnerability and response to sudden hydroclimatic shocks in both a statistical manner (e.g., Manning et al., 2017; Gao et al., 2021; Ludlow et al., 2023) and in a complementary qualitative manner as “revelatory crises” (Solway, 1994; Dove, 2014), in which tensions and vulnerabilities in political and economic systems are potentially exposed under pressure from sudden environmental variability (e.g., Ludlow and Crampsie, 2019; Huhtamaa et al., 2022; Ludlow et al., 2023).

For historical eruptions to act as tests or be studied as potential “revelatory” crises, knowledge of their dating alone is insufficient, particularly given the regional and seasonal variability of volcanic hydroclimatic impacts, and the sensitivity of these impacts to multiple variables such as the location, season, chemical composition, and height attained by volcanic ejecta (Robock, 2000; Cole-Dai, 2010; 770 Ludlow et al., 2013). Even where instrumental or natural archives are available, but especially where these are thin or absent, climate modelling can provide insights into the expected impacts for particular regions, seasons and related physical (e.g., riverine) systems (e.g., Toohey et al., 2016; McConnell et al., 2020; Mackay et al., 2022). This is true for modelling of idealized eruptions, but potentially even more so for models that produce “historical realizations” based upon actual forcing reconstructions (e.g., Tardif 775 et al., 2019).

In this context we have presented a modeling effort that explores the impacts of a unique eruption quartet during the (historically tumultuous) decade 168-158 BCE, with a focus on the Nile River basin. These target years are intermediate between the mid-Holocene and end of the preindustrial periods, and representative background climate conditions are necessary to investigate the climatic impact of such a 780 short-term forcing (Zanchettin et al., 2013). PMIP4 vegetation distributions (linearly interpolated for the 2.5ka period from the mid-Holocene (Otto-Bliesner et al., 2017) to the end of the preindustrial (taken as 1850) for the GISS ModelE2.1 (MATRIX) version (Kelley et al., 2020; Bauer et al., 2020)) were therefore used to improve GCM simulations without a fully dynamic vegetation implementation (Harrison et al., 2015). Vegetation-albedo feedbacks due to greater prevalence of arid shrubs/steppe over Africa and of 785 boreal forests over high latitudes were observed to induce a northward movement of the ITCZ over Africa (Sahara region) promoting a simulated rainfall increase of the order of 0.5-1.0 mm/day in the region (a response consistent with theoretical expectations and other estimates (e.g., Otterman, 1975; Charney, 1975; Claussen, 2009; Rachmayini et al., 2015; Pausata et al., 2016)).

The GISS ModelE2.1 simulated a strong shortwave and longwave global radiative forcing of -10 and +3.0 790 W/m², respectively, following the tropical eruption (E1) and a roughly equal forcing of -3.5 and +1.0 W/m², respectively, for each of the 3 extratropical eruptions (E2-E4). The peak net radiative volcanic forcing was calculated at -7.5 W/m² and -2.5 W/m² for the tropical and extratropical eruptions, respectively. The model calculated a global AOD at 550 nm of 0.22 and 0.1 after the tropical and

extratropical eruptions, respectively, and estimated a peak cooling of ~ 1.5 °C almost 12-months after the first eruption (E1), with the three consecutive eruptions then sustaining a surface cooling of about 1.0 °C for almost all of the 15 years modelled. The first eruption (E1) was 30% larger than Pinatubo and the GISS ModelE2.1 simulated proportionally stronger radiative impacts as compared to Pinatubo (for which see: Hansen et al., 1992; Robock and Mao, 1994; Parker et al., 1996; McCormick et al., 1995; Stenchikov, 2015). A detailed analysis of the impacts of volcanic aerosols on the chemical composition of the stratosphere was not part of this study.

The global hydrological cycle responded vigorously to the volcanically induced surface cooling in the GISS ModelE2.1, with a >1.0 mm/day decrease in rainfall observed over African, Indian, and Chinese regions during the summer monsoon season consecutively for 3 years after E1 (tropical) and for 2 years after each of the eruptions E2-E4 (extratropical northern hemispheric). Statistically significant decreases in rainfall over the major tropical northern hemisphere rain belt was also calculated by the model, as well as more broadly over higher latitudes for this hemisphere. Some smaller regions of positive rainfall anomalies were, however, simulated over the northern hemisphere mid-latitudes (land and ocean) around 30° N. These patterns of hydrological response are consistent with studies reporting changes in rainfall and large-scale atmospheric circulations (such as Hadley cell weakening) (e.g., Robock and Liu, 1994; Gillett et al., 2004; Trenberth and Dai, 2007; Crowley et al., 2008; Fischer et al., 2008; Joseph and Zeng, 2011; Timmreck, 2012; Iles et al., 2012, Haywood et al., 2013; Liu et al., 2016). However, we note that particularly on smaller spatial scales, as examined here, the variability in the modelled response as observed across our individual ensemble members may reduce the representativeness of the mean. The notable variability on display across our individual ensemble members, even to the quite substantial forcing represented by E1, also suggests that hydroclimatic responses on local to regional scales may depart from broader regional or hemispheric averages even after quite large volcanic forcings.

For the equatorial and northern African landmass specifically, the GISS ModelE2.1 produced a notable suppression of monsoon (JJAS) rainfall for all eruptions, E1-E4. The onset of this response can be observed in the JJAS season beginning with each eruption year itself, though the timing of the peak intensity and/or greatest spatial extent of this suppression varied (e.g., for E1 the greatest extent and peak intensity occurred for JJAS in Year 0, while for E2-E3 the peak intensity and greatest extent occurred in

Year 1, and for E4 in Year 0). The suppression centered (for all eruptions and each plotted post-eruption JJAS season, fig 10) around latitudes 10-15°N, where it ran in an east-west band that in some years was effectively contiguous across the continent (approx. 16°W to 52°E). There was, however, a tendency for
825 this response to be more marked and long-lived (into JJAS of Year 2, fig 10) in the central and eastern portions of this range, where it was statistically significant and could surpass 1 mm/day (up to 30-40% of climatology for control period).

Importantly, the regions of the most rapid onset, greatest persistence and intensity of response included Lake Tana (12°0'N 37°15'E) and the Ethiopian highlands that comprise the headwaters of the Blue Nile
830 and Atbara rivers and which supply most summer floodwater in Egypt (Melesse et al., 2011). This result is broadly consistent with CMIP5 model runs forced with large twentieth century eruptions (e.g., Iles and Hegerl, 2014; Manning et al., 2017). Annual river flow for the Nile River basin (fig 11) closely followed the patterns of decreased JJAS rainfall over the headwater region. Simulated river flow showed a deficit in the range of 15-40 km³/year up to 3 years following the modelled extratropical northern hemisphere
835 eruptions. Simulated variability in river discharge also increased 3/4-fold following the extratropical eruptions, but there is no way to tell which ensemble member best describes the historical conditions that actually occurred following the eruptions between 168 and 158 BCE. The large variability between ensembles and the statistical significance of the drying implies that Nile summer flooding might have been considerably lower than the simulated mean anomaly.

840 What is certain is that the scale and persistence of the hydroclimatic impacts implied by our modelling for the 168-158 BCE eruption quartet supports, to begin, inferences of poor Nile flooding in 166 and 161 BCE from scattered references in surviving written sources (Bonneau, 1971). These also identify 169 BCE as potentially experiencing poor flooding. This suggests (assuming sufficiently accurate ice-core dating (Sigl et al., 2015)) that the eruption quartet (the impacts of which are now better supported and
845 characterised by our modelling) may have compounded the stresses arising from this initial shock, contributing to what is long recognized as a tumultuous decade in Egyptian history. During the 6th Syrian War, Antiochus IV and his Seleukid army invaded Egypt twice. The first invasion occurred in 170 BCE and the second, more serious occupation, in 168 BCE. This takeover might indeed have re-shaped Mediterranean history had it not been averted by Roman diplomatic intervention (Hölbl, 2001). Internal

850 turmoil continued in Egypt in the 160s and 150s BCE, affecting both the capital Alexandria and the countryside. Surviving sources refer, for example, to “bad times and having been driven to every extremity owing to the price of wheat” in 168 BCE (*UPZ* 1 59; Bagnall and Derow, 2004, pp. 281-82), and it is known that by the middle of the decade an Egypt-wide agricultural crisis, described as a "calamity" was underway, driving Ptolemaic officials to near panic (*UPZ* 1 110, 165-164 BCE).

855 Manning et al. (2017) have identified dates of probable revolt onset in Ptolemaic history, with such onset dates identified in 168 BCE and 156 BCE, both coinciding closely with the dates of our eruption quartet. A study of the longevity and geography of these revolts is now of considerable interest. The surviving texts do not tell a complete story but scattered written references that imply a long persistence of revolt throughout the decade (Veisse 2004) are now rendered more explicable given the modelled persistence

860 of reduced temperatures and suppressed Nile summer flooding for more than a decade following the 168 BCE tropical eruption and the three following extratropical eruptions. More precisely delineating the political, military, economic and cultural pathways through which any volcanically induced hydroclimatic shock will have propagated is the subject of ongoing efforts to achieve a fuller understanding of the human-environmental entanglements of the 160s. Relatedly, open questions remain as to where along the

865 spectrum from proximate to ultimate causality (as per Gao et al., 2021) or necessary and sufficient conditions (as per White and Pei, 2020) hydroclimatic shocks lay in contributing to the revolts and other societal stresses that feature so prominently in Ptolemaic history.

Code/Data availability

870 Details to support the results in the manuscript is available as supplementary information is provided with the manuscript. Raw data and codes are available on request to author.

Acknowledgements

RS, KT, FL and JM acknowledge support by the National Science Foundation under Grant No. ICER-
875 1824770. ANL acknowledges institutional support from NASA GISS. Resources supporting this work were provided by the NASA High-End Computing (HEC) Program through the NASA Center for Climate Simulation (NCCS) at Goddard Space Flight Center. The authors thank for their input through multiple

discussions the project members and collaborators of the ICER-1824770 project, ‘Volcanism, Hydrology and Social Conflict: Lessons from Hellenistic and Roman-Era Egypt and Mesopotamia’. FL acknowledges support from the Trinity Center for Environmental Humanities. This paper benefited from discussion facilitated by the ‘Volcanic Impacts on Climate and Society’ (VICS) Working Group of PAGES.

Author’s contributions

FL and JM identified the study period in consultation with the other authors. RS, KT and ANL designed the model simulations. RS performed the simulations, created the figures in close collaboration with KT, ANL, FL and JM. RS wrote the first draft of the manuscript and RS, and FL led the writing of subsequent drafts. All authors contributed to the interpretation of results and the drafting of the text.

Competing interests

The authors declare no competing interests.

Short Summary

This study is a modelling effort to investigate hydroclimate impacts for the Nile River basin induced by a volcanic “quartet” of four closely spaced eruptions in ice-core volcanic chronology for the decade 168-158 BCE in a context to ancient Egyptian history. The NASA GISS ModelE simulated a strong response in sustained temperature reduction and suppressed monsoon rainfall over East Africa following these eruptions, leading to a deficit in Egypt’s agriculturally critical Nile summer flooding.

References

Aquila, V., Oman, L. D., Stolarski, R. S., Colarco, P. R., and Newman, P. A.: Dispersion of the volcanic sulfate cloud from a Mount Pinatubo–like eruption, 117, <https://doi.org/10.1029/2011JD016968>, 2012.

Aquila, V., Oman, L. D., Stolarski, R., Douglass, A. R., and Newman, P. A.: The Response of Ozone and Nitrogen Dioxide to the Eruption of Mt. Pinatubo at Southern and Northern Midlatitudes, 70, 894–900, <https://doi.org/10.1175/JAS-D-12-0143.1>, 2013.

- 905 Bauer, S. E., Wright, D. L., Koch, D., Lewis, E. R., and McGraw, R.: MATRIX (Multiconfiguration Aerosol TRacker of mIXing state): an aerosol microphysical module for global atmospheric models, 33, 2008.
- Bauer, S. E., Ault, A., and Prather, K. A.: Evaluation of aerosol mixing state classes in the GISS modelE-MATRIX climate model using single-particle mass spectrometry measurements, 118, 9834–9844, 910 <https://doi.org/10.1002/jgrd.50700>, 2013.
- Bauer, S. E., Tsigaridis, K., Faluvegi, G., Kelley, M., Lo, K. K., Miller, R. L., Nazarenko, L., Schmidt, G. A., and Wu, J.: Historical (1850–2014) Aerosol Evolution and Role on Climate Forcing Using the GISS ModelE2.1 Contribution to CMIP6, 12, e2019MS001978, <https://doi.org/10.1029/2019MS001978>, 2020.
- 915 Bell, B. 1975. ‘Climate and the History of Egypt: The Middle Kingdom’, *American Journal of Archaeology* 79(3): 223-69.
- Berhane, F., Zaitchik, B., and Dezfuli, A.: Subseasonal Analysis of Precipitation Variability in the Blue Nile River Basin, 27, 325–344, <https://doi.org/10.1175/JCLI-D-13-00094.1>, 2014.
- Blouin, J.: Defining and measuring tax planning aggressiveness, 67, 875–899, 920 <https://doi.org/10.17310/ntj.2014.4.06>, 2014.
- Bluth, G. J. S., Doiron, S. D., Schnetzler, C. C., Krueger, A. J., and Walter, L. S.: Global tracking of the SO₂ clouds from the June, 1991 Mount Pinatubo eruptions, 19, 151–154, <https://doi.org/10.1029/91GL02792>, 1992.
- Braconnot, P., Joussaume, S., Marti, O., and de Noblet, N.: Synergistic feedbacks from ocean and 925 vegetation on the African Monsoon response to Mid-Holocene insolation, 26, 2481–2484, <https://doi.org/10.1029/1999GL006047>, 1999.
- Brenna, H., Kutterolf, S., Mills, M. J., and Krüger, K.: The potential impacts of a sulfur- and halogen-rich supereruption such as Los Chocoyos on the atmosphere and climate, 20, 6521–6539, <https://doi.org/10.5194/acp-20-6521-2020>, 2020.
- 930 Broccoli, A. J., Dahl, K. A., and Stouffer, R. J.: Response of the ITCZ to Northern Hemisphere cooling, 33, <https://doi.org/10.1029/2005GL024546>, 2006.

- Butzer, K. W.: Early hydraulic civilization in Egypt: a study in cultural ecology, The University of Chicago Press, Chicago London, 134 pp., 1976.
- Butzer, K.W. 1984. 'Long-term Nile flood variation and political discontinuities in pharaonic Egypt', in: 935 J. Desmond Clark and S.A. Brandt (eds.), *From Hunters to Farmers: The Causes and Consequences of Food Production in Africa*, Berkeley, 102-12.
- Charney, J. G.: Dynamics of deserts and drought in the Sahel, 101, 193–202, <https://doi.org/10.1002/qj.49710142802>, 1975.
- Christiansen, B.: Volcanic Eruptions, Large-Scale Modes in the Northern Hemisphere, and the El Niño– 940 Southern Oscillation, 21, 910–922, <https://doi.org/10.1175/2007JCLI1657.1>, 2008.
- Chiang, J. C. H. and Bitz, C. M.: Influence of high latitude ice cover on the marine Intertropical Convergence Zone, *Climate Dynamics*, 25, 477–496, <https://doi.org/10.1007/s00382-005-0040-5>, 2005.
- Campbell, B. M. S. and Ludlow, F. (2020) "Climate, Disease and Society in Late-Medieval Ireland", *Proceedings of the Royal Irish Academy*, 120C, 159-252.
- 945 Claussen*, M.: Late Quaternary vegetation-climate feedbacks, 5, 203–216, <https://doi.org/10.5194/cp-5-203-2009>, 2009.
- Claussen, M., Brovkin, V., Ganopolski, A., Kubatzki, C., and Petoukhov, V.: Climate Change in Northern Africa: The Past is Not the Future, *Climatic Change*, 57, 99–118, <https://doi.org/10.1023/A:1022115604225>, 2003.
- 950 Cole- Dai J., 'Volcanoes and Climate', *WIREs Climate Change* , 1, 824– 39, 2010.
- Colose, C. M., LeGrande, A. N., and Vuille, M.: Hemispherically asymmetric volcanic forcing of tropical hydroclimate during the last millennium, *Earth Syst. Dynam.*, 7, 681–696, <https://doi.org/10.5194/esd-7-681-2016>, 2016.
- Crowley, T., GA, Z., Vinther, B., Udisti, R., Kreutzs, K., Cole-Dai, J., and Castellano, E.: Volcanism and 955 the Little Ice Age, *PAGES Newslett.*, 16, 22–23, <https://doi.org/10.1029/2002GL0166335>, 2008.
- D'Arrigo, R., Seager, R., Smerdon, J. E., LeGrande, A. N., and Cook, E. R.: The anomalous winter of 1783–1784: Was the Laki eruption or an analog of the 2009–2010 winter to blame?, 38, <https://doi.org/10.1029/2011GL046696>, 2011.

- Dogar, M. M.: Impact of Tropical Volcanic Eruptions on Hadley Circulation Using a High-Resolution
960 AGCM, 114, 1284, <https://doi.org/10.18520/cs/v114/i06/1284-1294>, 2018.
- Dove M. R.: *Anthropology of Climate Change* (Chichester, Wiley & Sons, 2014).
- Degroot, D., Anchukaitis, K., Bauch, M., Burnham, J., Carnegy, F., Cui, J., de Luna, K., Guzowski, P.,
Hambrecht, G., Huhtamaa, H., Izdebski, A., Kleemann, K., Moesswilde, E., Neupane, N., Newfield, T.,
965 Pei, Q., Xoplaki, E., and Zappia, N.: Towards a rigorous understanding of societal responses to climate
change. *Nature*, 591, 539–550, doi:10.1038/s41586-021-03190-2, 2021.
- Drake, B.L: ‘The Influence of Climatic Change on the Late Bronze Age Collapse and the Greek Dark
Ages’, *Journal of Archaeological Science* 39, pp.1862-1870, 2012
- A. Eckstein, Rome enters the Greek East: From Anarchy to Hierarchy in the Hellenistic Mediterranean,
230-170 BC. Blackwell, 2008.
- 970 English, J. M., Toon, O. B., and Mills, M. J.: Microphysical simulations of large volcanic eruptions:
Pinatubo and Toba, 118, 1880–1895, <https://doi.org/10.1002/jgrd.50196>, 2013.
- Eyring, V., Bony, S., Meehl, G. A., Senior, C. A., Stevens, B., Stouffer, R. J., and Taylor, K. E.: Overview
of the Coupled Model Intercomparison Project Phase 6 (CMIP6) experimental design and organization,
Geosci. Model Dev., 9, 1937–1958, <https://doi.org/10.5194/gmd-9-1937-2016>, 2016.
- 975 Fischer, E. M., Luterbacher, J., Zorita, E., Tett, S. F. B., Casty, C., and Wanner, H.: European climate
response to tropical volcanic eruptions over the last half millennium, 34,
<https://doi.org/10.1029/2006GL027992>, 2007.
- Fujiwara, M., Hibino, T., Mehta, S. K., Gray, L., Mitchell, D., and Anstey, J.: Global temperature
response to the major volcanic eruptions in multiple reanalysis data sets, *Atmos. Chem. Phys.*, 15, 13507–
980 13518, <https://doi.org/10.5194/acp-15-13507-2015>, 2015.
- Gao, F., Morisette, J. T., Wolfe, R. E., Ederer, G., Pedelty, J., Masuoka, E., Myneni, R., Tan, B., and
Nightingale, J.: An Algorithm to Produce Temporally and Spatially Continuous MODIS-LAI Time
Series, 5, 60–64, <https://doi.org/10.1109/LGRS.2007.907971>, 2008.
- Gao, C., Ludlow, F., Matthews, A., Stine, A. R., Robock, A., Pan, Y., Breen, R. and Sigl. M. (2021)
985 “Volcanic Climate Impacts Can Act as Ultimate and Proximate Causes of Chinese Dynastic Collapse”,
Communications Earth & Environment, 2, Article Number: 234. DOI: 10.1038/s43247-021-00284-7

- Gillett, N. P., Weaver, A. J., Zwiers, F. W., and Wehner, M. F.: Detection of volcanic influence on global precipitation, 31, <https://doi.org/10.1029/2004GL020044>, 2004.
- 990 Guillet, S., Corona, C., Ludlow, F., Oppenheimer, C., and Stoffel, M.: Climatic and societal impacts of a “forgotten” cluster of volcanic eruptions in 1108-1110 CE, *Sci Rep*, 10, 6715, <https://doi.org/10.1038/s41598-020-63339-3>, 2020.
- Guo, S., Bluth, G. J. S., Rose, W. I., Watson, I. M., and Prata, A. J.: Re-evaluation of SO₂ release of the 15 June 1991 Pinatubo eruption using ultraviolet and infrared satellite sensors, 5, <https://doi.org/10.1029/2003GC000654>, 2004.
- 995 Gu, G. and Adler, R. F.: Precipitation and Temperature Variations on the Interannual Time Scale: Assessing the Impact of ENSO and Volcanic Eruptions, 24, 2258–2270, <https://doi.org/10.1175/2010JCLI3727.1>, 2011.
- Graf, H.-F.: Arctic radiation deficit and climate variability, *Climate Dynamics*, 7, 19–28, <https://doi.org/10.1007/BF00204818>, 1992.
- 1000 Graft, H.-F., Kirchner, I., Robock, A., and Schult, I.: Pinatubo eruption winter climate effects: model versus observations, *Climate Dynamics*, 9, 81–93, <https://doi.org/10.1007/BF00210011>, 1993.
- Graf, H.-F., Li, Q., and Giorgetta, M. A.: Volcanic effects on climate: revisiting the mechanisms, 7, 4503–4511, <https://doi.org/10.5194/acp-7-4503-2007>, 2007.
- Grainger, J. *The Syrian Wars* (Brill, 2010).
- 1005 Hansen, J. E., Lacis, A. A., Lee, P., and Wang, W.-C.: Climatic Effects of Atmospheric Aerosols, 338, 575–587, <https://doi.org/10.1111/j.1749-6632.1980.tb17151.x>, 1980.
- Hansen, J., Lacis, A., Ruedy, R., and Sato, M.: Potential climate impact of Mount Pinatubo eruption, 19, 215–218, <https://doi.org/10.1029/91GL02788>, 1992.
- Hassan, F. A.: Nile Floods and Political Disorder in Early Egypt, in: *Third Millennium BC Climate Change and Old World Collapse*, Berlin, Heidelberg, 1–23, https://doi.org/10.1007/978-3-642-60616-8_1, 1997b.
- 1010 Hassan, F.A. 1997a. ‘The Dynamics of a Riverine Civilization: A Geoarchaeological Perspective on the Nile Valley, Egypt’, *World Archaeology* 29(1): 51-74.

- Hassan, F. A.: Extreme Nile floods and famines in Medieval Egypt (AD 930–1500) and their climatic implications, *Quaternary International*, 173–174, 101–112, <https://doi.org/10.1016/j.quaint.2007.06.001>, 2007.
- Harrison, S. P., Bartlein, P. J., Izumi, K., Li, G., Annan, J., Hargreaves, J., Braconnot, P., and Kageyama, M.: Evaluation of CMIP5 palaeo-simulations to improve climate projections, *Nature Clim Change*, 5, 735–743, <https://doi.org/10.1038/nclimate2649>, 2015.
- Haywood, J. M., Jones, A., Bellouin, N., and Stephenson, D.: Asymmetric forcing from stratospheric aerosols impacts Sahelian rainfall, *Nature Clim Change*, 3, 660–665, <https://doi.org/10.1038/nclimate1857>, 2013.
- Hewitt, C. D. and Mitchell, J. F. B.: A fully coupled GCM simulation of the climate of the mid-Holocene, 25, 361–364, <https://doi.org/10.1029/97GL03721>, 1998.
- Hölbl, G. A History of the Ptolemaic Empire (Routledge, 2001).
- Hsiang, S.M., Burke, M. (2014) Climate, conflict, and social stability: what does the evidence say? *Climatic Change*, 123, 39–55.
- Huhtamaa, H., Stoffel, M. and Corona, C. (2022). Recession or resilience? Long-range socioeconomic consequences of the 17th-century volcanic eruptions in northern Fennoscandia, *Climate of the Past Discussions*. <https://doi.org/10.5194/cp-2021-147>.
- Ide, T. (2017), Research methods for exploring the links between climate change and conflict. *WIREs Clim. Change*, 8: e456. <https://doi.org/10.1002/wcc.456>.
- Iles, C. E., Hegerl, G. C., Schurer, A. P., and Zhang, X.: The effect of volcanic eruptions on global precipitation, 118, 8770–8786, <https://doi.org/10.1002/jgrd.50678>, 2013.
- Iles, C. E. and Hegerl, G. C.: The global precipitation response to volcanic eruptions in the CMIP5 models, *Environ. Res. Lett.*, 9, 104012, <https://doi.org/10.1088/1748-9326/9/10/104012>, 2014.
- Ito, G., Romanou, A., Kiang, N. Y., Faluvegi, G., Aleinov, I., Ruedy, R., Russell, G., Lerner, P., Kelley, M., and Lo, K.: Global Carbon Cycle and Climate Feedbacks in the NASA GISS ModelE2.1, 12, e2019MS002030, <https://doi.org/10.1029/2019MS002030>, 2020.
- Izdebski, A., Bloomfield, K., Eastwood, W. J., Fernandes, R., Fleitmann, D., Guzowski, P., Haldon, J., Ludlow, F., Luterbacher, J., Manning, J. G., Masi, A., Mordechai, L., Newfield, T., Stine, A. R., Senkul,

- C. and Xoplaki, E. (In Press, 2023), “The Emergence of Interdisciplinary Environmental History: Bridging the Gap between the Humanistic and Scientific Approaches to the Late Holocene,” *Annales*, 77 (2), 1-48.
- 1045 Jacobson, T. W. P., Yang, W., Vecchi, G. A., and Horowitz, L. W.: Impact of volcanic aerosol hemispheric symmetry on Sahel rainfall, *Clim Dyn*, 55, 1733–1758, <https://doi.org/10.1007/s00382-020-05347-7>, 2020.
- Joseph, R. and Zeng, N.: Seasonally Modulated Tropical Drought Induced by Volcanic Aerosol, 24, 2045–2060, <https://doi.org/10.1175/2009JCLI3170.1>, 2011.
- 1050 Jungclaus, J. H., Lorenz, S. J., Timmreck, C., Reick, C. H., Brovkin, V., Six, K., Segschneider, J., Giorgetta, M. A., Crowley, T. J., Pongratz, J., Krivova, N. A., Vieira, L. E., Solanki, S. K., Klocke, D., Botzet, M., Esch, M., Gayler, V., Haak, H., Raddatz, T. J., Roeckner, E., Schnur, R., Widmann, H., Claussen, M., Stevens, B., and Marotzke, J.: Climate and carbon-cycle variability over the last millennium, *Clim. Past*, 6, 723–737, <https://doi.org/10.5194/cp-6-723-2010>, 2010.
- 1055 Kelley, M., Schmidt, G. A., Nazarenko, L. S., Bauer, S. E., Ruedy, R., Russell, G. L., Ackerman, A. S., Aleinov, I., Bauer, M., Bleck, R., Canuto, V., Cesana, G., Cheng, Y., Clune, T. L., Cook, B. I., Cruz, C. A., Genio, A. D. D., Elsaesser, G. S., Faluvegi, G., Kiang, N. Y., Kim, D., Lacis, A. A., Leboissetier, A., LeGrande, A. N., Lo, K. K., Marshall, J., Matthews, E. E., McDermid, S., Mezuman, K., Miller, R. L., Murray, L. T., Oinas, V., Orbe, C., García-Pando, C. P., Perlwitz, J. P., Puma, M. J., Rind, D., Romanou, 1060 A., Shindell, D. T., Sun, S., Tausnev, N., Tsigaridis, K., Tselioudis, G., Weng, E., Wu, J., and Yao, M.-S.: GISS-E2.1: Configurations and Climatology, 12, e2019MS002025, <https://doi.org/10.1029/2019MS002025>, 2020.
- Kiang, N. Y.: Description of the NASA GISS vegetation dynamics model Tech. rep. NASA, 2012
- Khodri, M., Izumo, T., Vialard, J., Janicot, S., Cassou, C., Lengaigne, M., Mignot, J., Gastineau, G., 1065 Guilyardi, E., Lebas, N., Robock, A., and McPhaden, M. J.: Tropical explosive volcanic eruptions can trigger El Niño by cooling tropical Africa, *Nat Commun*, 8, 778, <https://doi.org/10.1038/s41467-017-00755-6>, 2017.
- Kilian, M., Brinkop, S., and Jöckel, P.: Impact of the eruption of Mt Pinatubo on the chemical composition of the stratosphere, 20, 11697–11715, <https://doi.org/10.5194/acp-20-11697-2020>, 2020.

- 1070 Kim, Y., Moorcroft, P. R., Aleinov, I., Puma, M. J., and Kiang, N. Y.: Variability of phenology and fluxes of water and carbon with observed and simulated soil moisture in the Ent Terrestrial Biosphere Model (Ent TBM version 1.0.1.0.0), *Biogeosciences*, <https://doi.org/10.5194/gmdd-8-5809-2015>, 2015.
- Kirtman, B., Power, S. B., Adedoyin, A. J., Boer, G. J., Bojariu, R., Camilloni, I., Doblas-Reyes, F., Fiore, A. M., Kimoto, M., Meehl, G., Prather, M., Sarr, A., Schar, C., Sutton, R., van Oldenborgh, G. J., Vecchi, 1075 G., and Wang, H.-J.: Chapter 11 - Near-term climate change: Projections and predictability, edited by: IPCC, Cambridge University Press, Cambridge, 2013.
- Klock D: Assessing the uncertainty in climate sensitivity, Report on Earth System Science 95, Max Plank Institute of Meteorology ISSN 1614-1199, 87pp, Phd Thesis 2011.
- Knapp, A.B. and Manning, S.W. : ‘Crisis in Context: The End of the Late Bronze Age in the Eastern 1080 Mediterranean’, *American Journal of Archaeology* 120 pp.99-149, 2016.
- Kostić, S., Stojković, M., Prohaska, S., and Vasović, N.: Modeling of river flow rate as a function of rainfall and temperature using response surface methodology based on historical time series, *Journal of Hydroinformatics*, 18, 651–665, <https://doi.org/10.2166/hydro.2016.153>, 2016.
- Kutzbach, J., Bonan, G., Foley, J., and Harrison, S. P.: Vegetation and soil feedbacks on the response of 1085 the African monsoon to orbital forcing in the early to middle Holocene, *Nature*, 384, 623–626, <https://doi.org/10.1038/384623a0>, 1996.
- Kutzbach, J. E. and Liu, Z.: Response of the African Monsoon to Orbital Forcing and Ocean Feedbacks in the Middle Holocene, 278, 440–443, <https://doi.org/10.1126/science.278.5337.440>, 1997.
- Labitzke, K. and McCormick, M. P.: Stratospheric temperature increases due to Pinatubo aerosols, 19, 1090 207–210, <https://doi.org/10.1029/91GL02940>, 1992.
- Lacis, A., Hansen, J., and Sato, M.: Climate forcing by stratospheric aerosols, *Geophys. Res. Lett.*, 19, 1607–1610, <https://doi.org/10.1029/92GL01620>, 1992.
- Larrasoaña, J. C., Roberts, A. P., and Rohling, E. J.: Dynamics of Green Sahara Periods and Their Role in Hominin Evolution, *PLOS ONE*, 8, e76514, <https://doi.org/10.1371/journal.pone.0076514>, 2013.
- 1095 LeGrande, A. N., Tsigaridis, K., and Bauer, S. E.: Role of atmospheric chemistry in the climate impacts of stratospheric volcanic injections, *Nature Geosci*, 9, 652–655, <https://doi.org/10.1038/ngeo2771>, 2016.

- Liu, F., Chai, J., Wang, B., Liu, J., Zhang, X., and Wang, Z.: Global monsoon precipitation responses to large volcanic eruptions, *Sci Rep*, 6, 24331, <https://doi.org/10.1038/srep24331>, 2016.
- Ludlow, F., Stine, A. R., Leahy, P., Murphy, E., Mayewski, P., Taylor, D., Killen, J., Baillie, M.,
1100 Hennessy, M. and Kiely, G. “Medieval Irish Chronicles Reveal Persistent Volcanic Forcing of Severe Winter Cold Events, 431-1649 CE”, *Environmental Research Letters*, 8 (2), L024035, doi:10.1088/1748-9326/8/2/024035, 2013.
- Ludlow, F. & Manning, J. G. in *Climate Change and Ancient Societies in Europe and the Near East: Diversity in Collapse and Resilience* (eds Erdkamp, P., Manning, J. G. and Verboven K.) 301-320
1105 (Palgrave Macmillan, 2021).
- Ludlow, F. & Manning, J. G. in *Revolt and resistance in the Ancient Classical World and the Near East: The crucible of empire* (eds Collins, J. J. & Manning, J. G.) 154–171 (Brill, 2016)
- Ludlow, F. and Travis, C. (2019) “STEAM Approaches to Climate Change, Extreme Weather and Social-Political Conflict”, In: de la Garza, A. & Travis, C. (eds.), *The STEAM Revolution: Transdisciplinary*
1110 *Approaches to Science, Technology, Engineering, Arts, Humanities and Mathematics*. New York: Springer, 33-65.
- Ludlow, F., Kostick, C. and Morris, C. in *The Cambridge World History of Genocide* (eds Ben Kiernan, Tracy Maria Lemos and Tristan Taylor) (Cambridge University Press, In Press, 2023).
- Ludlow, F. and Crampsie, A.: “Climate, Debt and Conflict: Environmental History as a New Direction in
1115 *Understanding Early Modern Ireland*”, In: Sarah Covington, Vincent Carey and Valerie McGowan-Doyle (eds.), *Early Modern Ireland: New Sources, Methods, and Directions*. London: Routledge, 269-300, 2019.
- Ljungqvist, F. C., Seim, A. and Huhtamaa, H.: Climate and Society in European History. *WIRE’s Climate Change*, 12, e691. <https://doi.org/10.1002/wcc.691>.
- 1120 Mackay, H., Plunkett, G., Jensen, B., Aubry, T., Corona, C., Mi Kim, W., Toohey, M., Sigl, M., Stoffel, M., Anchukaitis, K., Raible, C., Bolton, M., Manning, J., Newfield, T., di Cosmo, N., Ludlow, F., Kostick, C., Yang, Z., Coyle McClung, L., Amesbury, M., Monteath, A., Hughes, P., Langdon, P., Charman, D., Booth, R., Davies, K., Blundell, A. and Swindles, G. (2022), “The 852/3 CE Mount Churchill Eruption: Examining the Potential Climatic and Societal Impacts and the Timing of the Medieval Climate Anomaly

- 1125 in the North Atlantic Region”, *Climate of the Past*, 18, 1475-1508. <https://doi.org/10.5194/cp-18-1475-2022>.
- Manning, J. G. *Land and Power in Ptolemaic Egypt: The Structure of Land Tenure* (Cambridge University Press, 2003).
- Manning, J. G., Ludlow, F., Stine, A. R., Boos, W. R., Sigl, M., and Marlon, J. R.: Volcanic suppression
1130 of Nile summer flooding triggers revolt and constrains interstate conflict in ancient Egypt, *Nat Commun*, 8, 900, <https://doi.org/10.1038/s41467-017-00957-y>, 2017.
- J. G. Manning, *The Open Sea: The Economic Life of the Ancient Mediterranean World from the Iron Age to the Rise of Rome* (Princeton: Princeton University Press, 2018)
- McCormick, M. P., Thomason, L. W., and Trepte, C. R.: Atmospheric effects of the Mt Pinatubo eruption,
1135 *Nature*, 373, 399–404, <https://doi.org/10.1038/373399a0>, 1995.
- McCormick, M. History's changing climate: Climate science, genomics and the emerging consilient approach to interdisciplinary history,” *Journal of Interdisciplinary History* 42 (2011): 252-73.
- McCormick, M. 2013. ‘What climate science, Ausonius, Nile floods, rye, and thatch tell us about the environmental history of the Roman Empire’, in 61-88.
- 1140 McCormick, M. Climates of History, *Histories of Climate: From History to Archaeoscience*, *Journal of Interdisciplinary History*, 50 (2019): 3–30.
- McConnell, J. R., Sigl, M., Plunkett, G., Burke, A., Kim, W. M., Raible, C. C., Wilson, A. I., Manning, J. G., Ludlow, F., Chellman, N. J., Innes, H. M., Yang, Z., Larsen, J. F., Schaefer, J. R., Kipfstuhl, S., Mojtabavi, S., Wilhelms, F., Opel, T., Meyer, H., and Steffensen, J. P.: Extreme climate after massive
1145 eruption of Alaska’s Okmok volcano in 43 BCE and effects on the late Roman Republic and Ptolemaic Kingdom, *Proc Natl Acad Sci USA*, 117, 15443–15449, <https://doi.org/10.1073/pnas.2002722117>, 2020.
- McGing, B. C. Revolt Egyptian style: Internal opposition to Ptolemaic rule. *Arch. Papyrusforschung* 43, 274–277 (1997).
- Mikhail, A. 2015. ‘Ottoman Iceland: A climate history’, *Environmental History* 20: 262–284.
- 1150 Melesse, A. M. (Ed.): *Nile River Basin*, Springer Netherlands, Dordrecht, <https://doi.org/10.1007/978-94-007-0689-7>, 2011.

- Myhre, G., D. Shindell, F.-M. Bréon, W. Collins, J. Fuglestedt, J. Huang, D. Koch, J.-F. Lamarque, D. Lee, B. Mendoza, T. Nakajima, A. Robock, G. Stephens, T. Takemura, and H. Zhang,: Anthropogenic and natural radiative forcing. In *Climate Change 2013: The Physical Science Basis. Contribution of Working Group I to the Fifth Assessment Report of the Intergovernmental Panel on Climate Change*. T.F. Stocker, D. Qin, G.-K. Plattner, M. Tignor, S.K. Allen, J. Doschung, A. Nauels, Y. Xia, V. Bex, and P.M. Midgley, Eds. Cambridge University Press, pp. 659-740, doi:10.1017/CBO9781107415324.018, 2013
- 1155 Myneni, R. B., Hoffman, S., Knyazikhin, Y., Privette, J. L., Glassy, J., Tian, Y., Wang, Y., Song, X., Zhang, Y., Smith, G. R., Lotsch, A., Friedl, M., Morisette, J. T., Votava, P., Nemani, R. R., and Running, S. W.: Global products of vegetation leaf area and fraction absorbed PAR from year one of MODIS data, *Remote Sensing of Environment*, 83, 214–231, [https://doi.org/10.1016/S0034-4257\(02\)00074-3](https://doi.org/10.1016/S0034-4257(02)00074-3), 2002.
- Oman, L., Robock, A., Stenchikov, G., Schmidt, G. A., and Ruedy, R.: Climatic response to high-latitude volcanic eruptions, 110, <https://doi.org/10.1029/2004JD005487>, 2005.
- Oman, L., Robock, A., Stenchikov, G. L., Thordarson, T., Koch, D., Shindell, D. T., and Gao, C.: 1165 Modeling the distribution of the volcanic aerosol cloud from the 1783–1784 Laki eruption, *J. Geophys. Res.*, 111, D12209, <https://doi.org/10.1029/2005JD006899>, 2006.
- Otterman, J.: Baring High-Albedo Soils by Overgrazing: A Hypothesized Desertification Mechanism, 186, 531–533, <https://doi.org/10.1126/science.186.4163.531>, 1974.
- Otto-Bliesner, B. L., Braconnot, P., Harrison, S. P., Lunt, D. J., Abe-Ouchi, A., Albani, S., Bartlein, P. J., 1170 Capron, E., Carlson, A. E., Dutton, A., Fischer, H., Goelzer, H., Govin, A., Haywood, A., Joos, F., LeGrande, A. N., Lipscomb, W. H., Lohmann, G., Mahowald, N., Nehrbass-Ahles, C., Pausata, F. S. R., Peterschmitt, J.-Y., Phipps, S. J., Renssen, H., and Zhang, Q.: The PMIP4 contribution to CMIP6 – Part 2: Two interglacials, scientific objective and experimental design for Holocene and Last Interglacial simulations, 10, 3979–4003, <https://doi.org/10.5194/gmd-10-3979-2017>, 2017.
- 1175 PAGES 2k Consortium, Continental-scale temperature variability during the past two millennia, *Nature Geoscience*, 6, 339-346 2013.
- PAGES 2k Consortium, A global database for temperature reconstructions of the Common Era, *Scientific Data*, 4:170088 | DOI: 10.1038/sdata.2017.88

- PAGES Hydro2k Consortium: Comparing proxy and model estimates of hydroclimate variability and
1180 change over the Common Era, 13, 1851–1900, <https://doi.org/10.5194/cp-13-1851-2017>, 2017.
- Parker, D. E., Wilson, H., Jones, P. D., Christy, J. R., and Folland, C. K.: The Impact of Mount Pinatubo
on World-Wide Temperatures, 16, 487–497, [https://doi.org/10.1002/\(SICI\)1097-0088\(199605\)16:5<487::AID-JOC39>3.0.CO;2-J](https://doi.org/10.1002/(SICI)1097-0088(199605)16:5<487::AID-JOC39>3.0.CO;2-J), 1996.
- Pausata, F. S. R., Chafik, L., Caballero, R., and Battisti, D. S.: Impacts of high-latitude volcanic eruptions
1185 on ENSO and AMOC, *Proc Natl Acad Sci USA*, 112, 13784–13788, <https://doi.org/10.1073/pnas.1509153112>, 2015.
- Pausata, F. S. R., Messori, G., and Zhang, Q.: Impacts of dust reduction on the northward expansion of
the African monsoon during the Green Sahara period, *Earth and Planetary Science Letters*, 434, 298–307,
<https://doi.org/10.1016/j.epsl.2015.11.049>, 2016.
- 1190 Peterson, L. C., Haug, G. H., Hughen, K. A., and Röhl, U.: Rapid Changes in the Hydrologic Cycle of
the Tropical Atlantic During the Last Glacial, <https://doi.org/10.1126/science.290.5498.1947>, 2000.
- Pitari, G. and Mancini, E.: Short-term climatic impact of the 1991 volcanic eruption of Mt. Pinatubo and
effects on atmospheric tracers, *Nat. Hazards Earth Syst. Sci.*, 2, 91–108, <https://doi.org/10.5194/nhess-2-91-2002>, 2002.
- 1195 Pitari, G., Cionni, I., Di Genova, G., Visioni, D., Gandolfi, I., and Mancini, E.: Impact of Stratospheric
Volcanic Aerosols on Age-of-Air and Transport of Long-Lived Species, 7, 149,
<https://doi.org/10.3390/atmos7110149>, 2016.
- Rachmayani, R., Prange, M., and Schulz, M.: North African vegetation–precipitation feedback in early
and mid-Holocene climate simulations with CCSM3-DGVM, *Clim. Past*, 11, 175–185,
1200 <https://doi.org/10.5194/cp-11-175-2015>, 2015. <https://doi.org/10.5194/cp-11-175-2015>, 2015.
- Rao, M. P., Cook, B. I., Cook, E. R., D’Arrigo, R. D., Krusic, P. J., Anchukaitis, K. J., LeGrande, A. N.,
Buckley, B. M., Davi, N. K., Leland, C., and Griffin, K. L.: European and Mediterranean hydroclimate
responses to tropical volcanic forcing over the last millennium, 44, 5104–5112,
<https://doi.org/10.1002/2017GL073057>, 2017.
- 1205 Read, W. G., Froidevaux, L., and Waters, J. W.: Microwave limb sounder measurement of stratospheric
SO₂ from the Mt. Pinatubo Volcano, 20, 1299–1302, <https://doi.org/10.1029/93GL00831>, 1993.

- Robock, A.: Volcanic eruptions and climate, 38, 191–219, <https://doi.org/10.1029/1998RG000054>, 2000.
- Robock, A. and Mao, J.: Winter warming from large volcanic eruptions, *Geophys. Res. Lett.*, 19, 2405–2408, <https://doi.org/10.1029/92GL02627>, 1992.
- 1210 Robock, A. and Liu, Y.: The Volcanic Signal in Goddard Institute for Space Studies Three-Dimensional Model Simulations, 7, 44–55, [https://doi.org/10.1175/1520-0442\(1994\)007<0044:TVSIGI>2.0.CO;2](https://doi.org/10.1175/1520-0442(1994)007<0044:TVSIGI>2.0.CO;2), 1994.
- Robock, A. and Mao, J.: The Volcanic Signal in Surface Temperature Observations, 8, 1086–1103, [https://doi.org/10.1175/1520-0442\(1995\)008<1086:TVSIST>2.0.CO;2](https://doi.org/10.1175/1520-0442(1995)008<1086:TVSIST>2.0.CO;2), 1995.
- 1215 Roger S. Bagnall and Peter Derow, *Historical Sources in Translation. The Hellenistic Period*. New Edition, Blackwell, 2004.
- Roller, D. W. *Cleaopatra: A Biography* (Oxford University Press, 2010).
- Sabzevari, A. A., Zarenistanak, M., Tabari, H., and Moghimi, S.: Evaluation of precipitation and river discharge variations over southwestern Iran during recent decades, *J Earth Syst Sci*, 124, 335–352, 1220 <https://doi.org/10.1007/s12040-015-0549-x>, 2015.
- Russell, P. B., Livingston, J. M., Pueschel, R. F., Bauman, J. J., Pollack, J. B., Brooks, S. L., Hamill, P., Thomason, L. W., Stowe, L. L., Deshler, T., Dutton, E. G., and Bergstrom, R. W.: Global to microscale evolution of the Pinatubo volcanic aerosol derived from diverse measurements and analyses, 101, 18745–18763, <https://doi.org/10.1029/96JD01162>, 1996.
- 1225 Schmidt, A., Carslaw, K. S., Mann, G. W., Wilson, M., Breider, T. J., Pickering, S. J., and Thordarson, T.: The impact of the 1783–1784 AD Laki eruption on global aerosol formation processes and cloud condensation nuclei, 10, 6025–6041, <https://doi.org/10.5194/acp-10-6025-2010>, 2010.
- Schmidt, G. A., Ruedy, R., Hansen, J. E., Aleinov, I., Bell, N., Bauer, M., Bauer, S., Cairns, B., Canuto, V., Cheng, Y., Del Genio, A., Faluvegi, G., Friend, A. D., Hall, T. M., Hu, Y., Kelley, M., Kiang, N. Y., 1230 Koch, D., Lacis, A. A., Lerner, J., Lo, K. K., Miller, R. L., Nazarenko, L., Oinas, V., Perlwitz, J., Perlwitz, J., Rind, D., Romanou, A., Russell, G. L., Sato, M., Shindell, D. T., Stone, P. H., Sun, S., Tausnev, N., Thresher, D., and Yao, M.-S.: Present-Day Atmospheric Simulations Using GISS ModelE: Comparison to In Situ, Satellite, and Reanalysis Data, 19, 153–192, <https://doi.org/10.1175/JCLI3612.1>, 2006.

- Schmidt, G. A., Jungclaus, J. H., Ammann, C. M., Bard, E., Braconnot, P., Crowley, T. J., Delaygue, G.,
1235 Joos, F., Krivova, N. A., Muscheler, R., Otto-Bliesner, B. L., Pongratz, J., Shindell, D. T., Solanki, S. K.,
Steinhilber, F., and Vieira, L. E. A.: Climate forcing reconstructions for use in PMIP simulations of the
last millennium (v1.0), *Geosci. Model Dev.*, 4, 33–45, <https://doi.org/10.5194/gmd-4-33-2011>, 2011.
- Schmidt, G. A., Kelley, M., Nazarenko, L., Ruedy, R., Russell, G. L., Aleinov, I., Bauer, M., Bauer, S.
E., Bhat, M. K., Bleck, R., Canuto, V., Chen, Y.-H., Cheng, Y., Clune, T. L., Del Genio, A., de Fainchtein,
1240 R., Faluvegi, G., Hansen, J. E., Healy, R. J., Kiang, N. Y., Koch, D., Lacis, A. A., LeGrande, A. N.,
Lerner, J., Lo, K. K., Matthews, E. E., Menon, S., Miller, R. L., Oinas, V., Oloso, A. O., Perlwitz, J. P.,
Puma, M. J., Putman, W. M., Rind, D., Romanou, A., Sato, M., Shindell, D. T., Sun, S., Syed, R. A.,
Tausnev, N., Tsigaridis, K., Unger, N., Voulgarakis, A., Yao, M.-S., and Zhang, J.: Configuration and
assessment of the GISS ModelE2 contributions to the CMIP5 archive: GISS MODEL-E2 CMIP5
1245 SIMULATIONS, *J. Adv. Model. Earth Syst.*, 6, 141–184, <https://doi.org/10.1002/2013MS000265>, 2014.
- Said, R. 1993. *The River Nile: Geology, Hydrology and Utilization*. Oxford.
- Schneider, D. P., Ammann, C. M., Otto-Bliesner, B. L., and Kaufman, D. S.: Climate response to large,
high-latitude and low-latitude volcanic eruptions in the Community Climate System Model, 114,
<https://doi.org/10.1029/2008JD011222>, 2009.
- 1250 Schneider A. W. and Adali, S.F. : “No Harvest was Reaped’: Demographic and Climatic Factors in the
Decline of the Neo-Assyrian Empire’, *Climatic Change* 127, pp.435-446, 2014.
- Schnetzler, C. C., Krueger, A. J., Bluth, G. S., Sprod, I. E., and Walter, L. S.: Comment on the Paper “The
atmospheric SO₂ budget for Pinatubo derived from NOAA-11 SBUV/2 spectral data” by R. D. McPeters,
22, 315–316, <https://doi.org/10.1029/94GL02406>, 1995.
- 1255 Segele, Z. T., Lamb, P. J., and Leslie, L. M.: Large-scale atmospheric circulation and global sea surface
temperature associations with Horn of Africa June–September rainfall, 29, 1075–1100,
<https://doi.org/10.1002/joc.1751>, 2009.
- Shindell, D. T.: Dynamic winter climate response to large tropical volcanic eruptions since 1600, *J.*
Geophys. Res., 109, D05104, <https://doi.org/10.1029/2003JD004151>, 2004.
- 1260 Shindell, D. T., Faluvegi, G., Unger, N., Aguilar, E., Schmidt, G. A., Koch, D. M., Bauer, S. E., and
Miller, R. L.: Simulations of preindustrial, present-day, and 2100 conditions in the NASA GISS

- composition and climate model G-PUCCINI, 6, 4427–4459, <https://doi.org/10.5194/acp-6-4427-2006>, 2006.
- 1265 Sigl, M., Winstrup, M., McConnell, J. R., Welten, K. C., Plunkett, G., Ludlow, F., Büntgen, U., Caffee, M., Chellman, N., Dahl-Jensen, D., Fischer, H., Kipfstuhl, S., Kostick, C., Maselli, O. J., Mekhaldi, F., Mulvaney, R., Muscheler, R., Pasteris, D. R., Pilcher, J. R., Salzer, M., Schüpbach, S., Steffensen, J. P., Vinther, B. M., and Woodruff, T. E.: Timing and climate forcing of volcanic eruptions for the past 2,500 years, *Nature*, 523, 543–549, <https://doi.org/10.1038/nature14565>, 2015.
- 1270 Simard, M., Pinto, N., Fisher, J. B., and Baccini, A.: Mapping forest canopy height globally with spaceborne lidar, 116, <https://doi.org/10.1029/2011JG001708>, 2011.
- Singh, R. and AchutaRao, K.: Quantifying uncertainty in twenty-first century climate change over India, *Clim Dyn*, 52, 3905–3928, <https://doi.org/10.1007/s00382-018-4361-6>, 2019.
- Singh, R., LeGrande, A. N., and Tsigaridis, K.: Influence of regional anthropogenic changes over Nile region on the climate system during the late Holocene (~2500 years before present), EGU General Assembly 2020, Online, 4–8 May 2020, EGU2020-12338, <https://doi.org/10.5194/egusphere-egu2020-12338>, 2020.
- 1275 Staunton-Sykes, J., Aubry, T. J., Shin, Y. M., Weber, J., Marshall, L. R., Luke Abraham, N., Archibald, A., and Schmidt, A.: Co-emission of volcanic sulfur and halogens amplifies volcanic effective radiative forcing, 21, 9009–9029, <https://doi.org/10.5194/acp-21-9009-2021>, 2021.
- 1280 Solway, J. S. : ‘Drought as a Revelatory Crisis: An Exploration of Shifting Entitlements and Hierarchies in the Kalahari, Botswana’, *Development and Change* 25, pp.471-495, 1994.
- Stenchikov, G.: Chapter 26 - The Role of Volcanic Activity in Climate and Global Change, in: *Climate Change (Second Edition)*, edited by: Letcher, T. M., Elsevier, Boston, 419–447, <https://doi.org/10.1016/B978-0-444-63524-2.00026-9>, 2016.
- 1285 Stoffel, M., Corona, C., Ludlow, F., Sigl, M., Huhtamaa, H., Garnier, E., Helama, S., Guillet, S., Crampsie, A., Kleemann, K., Camenisch, C., McConnell, J. and Gao, C. (In Review, 2022), “Climatic, Weather and Socio-Economic Conditions Corresponding with the mid-17th Century Eruption Cluster”, *Climate of the Past*.

- Swingedouw, D., Mignot, J., Ortega, P., Khodri, M., Menegoz, M., Cassou, C., and Hanquiez, V.: Impact
1290 of explosive volcanic eruptions on the main climate variability modes, *Global and Planetary Change*, 150,
24–45, <https://doi.org/10.1016/j.gloplacha.2017.01.006>, 2017.
- Sołtysiak, A. : ‘Drought and the Fall of Assyria: Quite Another Story’, *Climatic Change* 136, 2016,
pp.389-394, 2016.
- Tardif, R., Hakim, G.J., Perkins, W.A., Horlick, K.A., Erb, M.P., Emile-Geay, J., Anderson, D.M., Steig,
1295 E.J. & Noone, D. (2019). Last Millennium Reanalysis with an Expanded Proxy Database and Seasonal
Proxy Modeling, *Climate of the Past*, 15, pp. 1251-1273.
- Thordarson, T.: Atmospheric and environmental effects of the 1783–1784 Laki eruption: A review and
reassessment, *J. Geophys. Res.*, 108, 4011, <https://doi.org/10.1029/2001JD002042>, 2003.
- Tierney, J. E., Pausata, F. S. R., and deMenocal, P. B.: Rainfall regimes of the Green Sahara,
1300 <https://doi.org/10.1126/sciadv.1601503>, 2017.
- Timmreck, C., Lorenz, S. J., Crowley, T. J., Kinne, S., Raddatz, T. J., Thomas, M. A., and Jungclaus, J.
H.: Limited temperature response to the very large AD 1258 volcanic eruption, *Geophys. Res. Lett.*, 36,
L21708, <https://doi.org/10.1029/2009GL040083>, 2009.
- Timmreck, C., Graf, H.-F., Lorenz, S. J., Niemeier, U., Zanchettin, D., Matei, D., Jungclaus, J. H., and
1305 Crowley, T. J.: Aerosol size confines climate response to volcanic super-eruptions, 37,
<https://doi.org/10.1029/2010GL045464>, 2010.
- Timmreck, C.: Modeling the climatic effects of large explosive volcanic eruptions, 3, 545–564,
<https://doi.org/10.1002/wcc.192>, 2012.
- Tiwari, S., Ramos, R., Pausata, F. S. R., LeGrande, A. N., Griffiths, M. L., Beltrami, H., Chandan, D., de
1310 Vernal, A., Litchmore, D., Peltier, R., and Tabor, C. R.: Model performance in simulating the mid-
Holocene Green Sahara, EGU General Assembly 2022, Vienna, Austria, 23–27 May 2022, EGU22-3233,
<https://doi.org/10.5194/egusphere-egu22-3233>, 2022
- Toohey, M., Krüger, K., Niemeier, U., and Timmreck, C.: The influence of eruption season on the global
aerosol evolution and radiative impact of tropical volcanic eruptions, *Atmos. Chem. Phys.*, 11, 12351–
1315 12367, <https://doi.org/10.5194/acp-11-12351-2011>, 2011.

- Toohey, M. and Sigl, M.: Volcanic stratospheric sulfur injections and aerosol optical depth from 500 BCE to 1900 CE, 9, 809–831, <https://doi.org/10.5194/essd-9-809-2017>, 2017.
- Toohey, M., Krüger, K., Sigl, M., Stordal, F., and Svensen, H.: Climatic and societal impacts of a volcanic double event at the dawn of the Middle Ages, *Climatic Change*, 136, 401–412, <https://doi.org/10.1007/s10584-016-1648-7>, 2016.
- Toohey, M., Krüger, K., Schmidt, H., Timmreck, C., Sigl, M., Stoffel, M., and Wilson, R.: Disproportionately strong climate forcing from extratropical explosive volcanic eruptions, 12, 100–107, <https://doi.org/10.1038/s41561-018-0286-2>, 2019.
- Trepte, C. R. and Hitchman, M. H.: Tropical stratospheric circulation deduced from satellite aerosol data, *Nature*, 355, 626–628, <https://doi.org/10.1038/355626a0>, 1992.
- Travis, C., Holm, P., Ludlow, F., Kostick, C., McGovern, R. and Nicholls, J. (2022) “Cowboys, Cod, Climate and Conflict: Navigations in the Digital Environmental Humanities”, In: Travis, C., Legg, R., Bergmann, L., Crampsie, A. and Dixon, D. (eds.), *Routledge Handbook of the Digital Environmental Humanities*. London: Routledge, 17-39.
- Trenberth, K. E. and Dai, A.: Effects of Mount Pinatubo volcanic eruption on the hydrological cycle as an analog of geoengineering: PINATUBO AND THE HYDROLOGICAL CYCLE, *Geophys. Res. Lett.*, 34, <https://doi.org/10.1029/2007GL030524>, 2007.
- Vashisht, A., Zaitchik, B., and Gnanadesikan, A.: ENSO Teleconnection to Eastern African Summer Rainfall in Global Climate Models: Role of the Tropical Easterly Jet, 34, 293–312, <https://doi.org/10.1175/JCLI-D-20-0222.1>, 2021.
- Vashisht, A., Zaitchik, B., and Gnanadesikan, A.: ENSO Teleconnection to Eastern African Summer Rainfall in Global Climate Models: Role of the Tropical Easterly Jet, 34, 293–312, <https://doi.org/10.1175/JCLI-D-20-0222.1>, 2021.
- van Bavel, B.J.P., Curtis, D.R., Hannaford, M.J., Moatsos, M., Roosen, J., and Soens, T.: Climate and society in long-term perspective: Opportunities and pitfalls in the use of historical datasets, *Wires Clim. Change*, 10(6), e611, doi: 10.1002/wcc.611, 2019.
- Vehkamäki, H., Kulmala, M., Napari, I., Lehtinen, K. E. J., Timmreck, C., Noppel, M., and Laaksonen, A.: An improved parameterization for sulfuric acid–water nucleation rates for tropospheric and stratospheric conditions, 107, AAC 3-1-AAC 3-10, <https://doi.org/10.1029/2002JD002184>, 2002.

- 1345 Veïsse, A.-E.: Les révoltes égyptiennes: recherches sur les troubles intérieurs en Égypte du règne de Ptolémée III à la conquête romaine, Peeters, Leuven; Paris; Dudley, MA, 2004.
- Villmoare B., *The Evolution of Everything: The Patterns and Causes of Big History* (Cambridge University Press, 2022)
- Vörösmarty, CJ; Fekete, BM; Tucker, BA (1998): Global River Discharge, 1807-1991, V. 1.1 (RivDIS). Data set. Available on-line [<http://www.daac.ornl.gov>] from Oak Ridge National Laboratory Distributed
- 1350 Active Archive Center, Oak Ridge, Tennessee, U.S.A.
- Wahl, E. R., Diaz, H. F., Smerdon, J. E., and Ammann, C. M.: Late winter temperature response to large tropical volcanic eruptions in temperate western North America: Relationship to ENSO phases, *Global and Planetary Change*, 122, 238–250, <https://doi.org/10.1016/j.gloplacha.2014.08.005>, 2014.
- 1355 Wolfe, E. W., and Hoblitt R. P.: Overview of the eruptions, in *Fire and Mud: Eruptions and lahars of the Moun Pinatubo, Philippines*, edited by Newhall C.G. and Punongbayan, pp. 415-433, Univ of Wash. Press, Seattle.
- White, S. and Pei, Q. (2020). Attribution of historical societal impacts and adaptations to climate and extreme events: Integrating quantitative and qualitative perspectives. *Past Global Changes Magazine*, 28(2), 44-45.
- 1360 Xian, P. and Miller, R. L.: Abrupt Seasonal Migration of the ITCZ into the Summer Hemisphere, 65, 1878–1895, <https://doi.org/10.1175/2007JAS2367.1>, 2008.
- Zanchettin, D., Bothe, O., Graf, H. F., Lorenz, S. J., Luterbacher, J., Timmreck, C., and Jungclaus, J. H.: Background conditions influence the decadal climate response to strong volcanic eruptions, 118, 4090–4106, <https://doi.org/10.1002/jgrd.50229>, 2013.
- 1365 Zanchettin, D., Timmreck, C., Khodri, M., Schmidt, A., Toohey, M., Abe, M., Bekki, S., Cole, J., Fang, S.-W., Feng, W., Hegerl, G., Johnson, B., Lebas, N., LeGrande, A. N., Mann, G. W., Marshall, L., Rieger, L., Robock, A., Rubinetti, S., Tsigaridis, K., and Weierbach, H.: Effects of forcing differences and initial conditions on inter-model agreement in the VolMIP volc-pinatubo-full experiment, 1–39, <https://doi.org/10.5194/gmd-2021-372>, 2021.

1370